DEPARTMENT OF THE INTERIOR

U.S. GEOLOGICAL SURVEY

LABORATORY MEASUREMENTS OF VELOCITY-DEPENDENT FRICTIONAL STRENGTH

by

D. A. Lockner and J. D. Byerlee[1]

Open-File Report 86–417

[1]U.S. Geological Survey, 345 Middlefield Road
Menlo Park, California 94025

1986

ABSTRACT

A variety of experiments have been conducted in which the velocity dependence of the steady-state coefficient of friction μ_V^{ss} in geologic materials has been measured. These experimental results, obtained using a variety of test geometries and samples, are compared. A partial list of the parameters that can affect μ_V^{ss} includes normal stress, water content, temperature, surface roughness, gouge composition, absolute sliding rate, total strain, and test geometry. The physical mechanisms by which these parameters affect the coefficient of friction are, at present, only partially understood.

INTRODUCTION

There exists a growing interest in how the frictional strength of geologic materials depends on the rate of deformation. This rate dependence may have applications at low pressures in soil mechanics research related to slope stability and landslides. At higher pressures, rate dependence of frictional strength may be important in controlling the mode of deformation of active faults, *i.e.*, earthquakes or stable creep. In recent years, a class of friction laws has been developed in which the frictional strength of a surface is the result of its deformation rate history as retained by a so-called fading memory. This class of velocity- and displacement-dependent friction laws is discussed, for example, in *Dieterich* (1981), *Rice* (1983), and *Ruina* (1983), and is now being used to model earthquake cycles; the most recent example appearing in *Tse and Rice* (1986).

In this paper we will concern ourselves primarily with *experimental* evidence of the velocity dependence of shear strength and in particular the velocity dependence of steady-state shear strength. A relatively small number of measurements of these parameters have been performed and we will look at these results in some detail. Effects due to mineral composition, grain size, surface roughness, machine geometry and other parameters will be discussed.

DISCUSSION

Effective normal stress is the principle parameter controlling frictional shear strength of rock at pressures found in the Earth's crust. (Effective normal stress $\bar{\sigma}_n$ is the difference between normal stress σ_n and pore pressure.) In most of the relevant laboratory studies, pore pressure was 0, so that normal stress and effective normal stress were the same. Compiling strength data on a variety of rock types, *Byerlee* (1978) found that, with the exception of some weak clays, shear strength (τ) varied by less than 10 percent for a variety of rocks. $\tau - \sigma_n$ relations are in general nonlinear ($\tau - \sigma_n$ plots are typically concave downwards) and for most rocks can be approximated by

$$\tau = 0.85\,\sigma_n, \quad \sigma_n < 200 \text{ MPa}, \tag{1a}$$

and

$$\tau = 50 + 0.6\,\sigma_n[\text{MPa}], \quad \sigma_n > 200 \text{ MPa} \tag{1b}$$

At low normal stress, interlocking of grains and surface roughness are very important in controlling shear strength. As a result, large deviations from (1a) can exist on a case-by-case basis. However, with increasing normal stress, grain crushing becomes progressively

more important as a deformation mechanism and the initial conditions of the gouge and sliding surfaces become less important.

Velocity Dependence of Steady-State Coefficient of Friction

From (1) we find that for most rocks the coefficient of friction ($\mu \equiv \tau/\sigma_n$) can be approximated by

$$\mu = 0.85, \quad \sigma_n < 200 \text{ MPa} \tag{2a}$$

and

$$\mu = 0.6 + \frac{50}{\sigma_n} \text{ [MPa]}, \quad \sigma_n > 200 \text{ MPa} \tag{2b}$$

Although, at low normal stress in particular, large variability in μ can occur depending on the initial conditions of the gouge and sliding surfaces. By comparison, relative changes in μ due to changes in deformation rate are generally only a few percent.

In order to quantify the velocity dependence of μ, we make the following definitions. We first assume that if a fault surface is deformed at constant σ_n and constant velocity (V), a steady-state coefficient of friction (μ_V^{ss}) will be achieved. This quantity μ_V^{ss} is of central importance and requires further comment. While it is appealing to think that if a fault deforms at constant velocity and normal stress it will approach a time-invariant shear strength, such behavior has probably never been observed. For example even after 70 mm of deformation (averge shear strain $\gamma \simeq 500$) on flat, clean granite surfaces *Tullis and Weeks* (1986) reported slowly varying strength transients. In a ring shear experiment at approximately 0.7 MPa normal stress, *Mandl et al.* (1977) observed large local stress variations, even after 3,200 mm displacement ($\gamma > 50$). At present, little is known about the structure of active faults at depth, although they are generally not flat, parallel surfaces. *Wallace and Morris* (1979) and *Robertson* (1983) have noted a correlation between total deformation and fault width, indicating that faults continue to evolve with deformation. Furthermore, seismically active faults maintain their structural heterogeneity, even after kilometers of deformation. Heterogeneity would result in continual variation of local stresses as the fault structure evolves. The motivation for defining the quantity μ_V^{ss} stems from an assumption that steady-state shear strength is controlled, in part, by sliding velocity independent of other variables. A practical definition of μ_V^{ss} must therefore allow for changes in shear strength, due to effects other than velocity, that vary slowly over the displacements being studied. These other effects could include displacement-dependent strain hardening or time-dependent processes such as chemical reactions (mineral alterations) or time-dependent compaction. These processes can all affect shear strength and, if not properly accounted for, can be misinterpreted as velocity-dependent effects.

One classic type of experiment used to determine the velocity dependence of μ involves an abrupt change in velocity from an initial sliding rate V_1 to a final rate V_2. A typical result from such an experiment, with $V_2 > V_1$, is shown in Figure 1. In experiments of this type, μ almost always goes to a peak and then decays to $\mu_{V_2}^{ss}$. In a manner similar to

Dieterich (1981), we define a characteristic distance (d_r) required for μ to decay to $(1/e)b$ as shown in Figure 1. As in *Dieterich* (1981), we define the parameter

$$B \equiv \frac{\Delta \mu^{ss}}{\log_{10}(V_2/V_1)} \tag{3}$$

Thus, B represents the change in the steady-state coefficient of friction resulting from a decade change in sliding rate. If B is positive, the fault becomes stronger at faster sliding rates (velocity strengthening) and if B is negative, the fault becomes weaker at faster rates (velocity weakening). Nearly all of the reported values of B for a variety of geologic materials fall in the range -0.03 to +0.03. *Dieterich* (1981) suggested that the specific value of B results from competing processes of similar magnitude. In recent formulations (*i.e., Rice and Gu*, 1983; *Tullis and Weeks*, 1986), B is expressed as the difference of two other quantities

$$B = \ln(10)\frac{d\mu^{ss}}{d(\ln(V))} = \ln(10)(a-b) \tag{4}$$

where a expresses the instantaneous change in μ with respect to slip rate

$$a = \frac{\partial \mu_{\text{inst.}}}{\partial(\ln(V))} \tag{5}$$

and b expresses the transient change in μ (Figure 1). Correlations have been reported between the magnitudes of a, b and B and such parameters as grain size, surface roughness, σ_n, water content, and temperature. However, the physical mechanisms that are responsible for these correlations, are still poorly understood.

The sign and magnitude of B are thought to be important. Theoretical considerations (*Rice and Ruina*, 1983; *Rice*, 1983; and *Tse and Rice*, 1986) suggest that, under appropriate conditions, unstable slip can only occur when B is negative. Since it is not clear that these conditions for instability are satisfied on natural faults, knowledge of the sign of B is, at present, of limited value in predicting the modes of deformation that will occur in the Earth. At the same time, there now exists more laboratory data on B than any other velocity-dependent friction parameter. As a result, a comparison of the values of B that have been reported for various test conditions and geometries and for various geologic materials can provide some insight into the processes occurring on natural and artificial faults.

Experimental Determination of B

Different methods have been used to measure the parameter B. In one method (*Teufel and Logan*, 1978) identical samples are deformed at different rates and the corresponding strengths are compared. One drawback of this method is that shear strength from one sample to another is generally reproducable to only a few percent, which is of the same order as the velocity effects being studied. Secondly, if time-dependent effects such as

gouge compaction occur, they can be erroneously included with strength changes due to slip rate.

The most commonly used method for determining B, as previously described (Figure 1) is to sequentially alter the sliding rate of a single sample. Because a finite displacement is required for transients in shear strength to dissipate, this method requires extrapolation of steady-state shear strength over some distance. If the extrapolation distance is too short, strength transients will not have completely dissipated and the resulting determination of B will be too positive. If the distance is too long, extrapolation errors become too large. Also, if trends in the strength curve are changing with displacements, these measurement problems are compounded. Minimum distances for strength transients to dissipate ($\simeq d_r$) for granite (*e.g., Dieterich*, 1978, 1981; *Tullis and Weeks*, 1986; *Lockner et al.*, 1986 range from 10 μm (bare smooth surfaces and fine gouge) to 200 μm (rough surfaces, coarse gouge or high temperature).

We will now look at the reported values of the parameter B. In Figures 2 and 2a we have plotted nearly all of the available data for B in geologic materials as a function of normal stress. Information regarding the data in Figures 2 and 2a is presented in Table 1. Horizontal bars span the range of measurements in normal stress. Vertical bars represent approximately one standard deviation in B. Since these data appear in the literature in a variety of different forms, caution should be used in any comparisons. These figures are probably most useful in showing the general ranges of B that have been reported for the various conditions studied. At first glance, there are no obvious trends in the values of B shown in Figure 2. No strong correlation between B and σ_n exists. SB studied the largest range in normal stress. A least squares fit to their data resulted in $B = 0.0006 + 0.0031 \log_{10} \sigma_n$ [MPa] with a standard deviation of 0.004.

Variations in B due to composition—Measurements performed on clays (Sk), mudstones (Sc) and chlorite (Sh) (in Figure 2) all show similar, positive B. It should be noted, however, that *Skempton* (1985) also reported results of high velocity (200 to 12,000 μm/s) low normal stress experiments performed on clays and siltstones. At these faster shear rates, large values of B, both positive and negative, were observed. These effects seemed to be related to internal structural changes as well as changes in pore pressure resulting from dilatancy and compaction.

Shimamoto (1986) and *Shimamoto and Logan* (1986) have studied velocity effects of halite gouge sliding on sandstone at room temperature. They observed a wide range in B (not plotted in Figure 2 due to the complexity of the data set but shown, in part, in Figure 4j) correlated with normal stress and sliding rate. For normal stresses ranging from 15 to 340 MPa and sliding rates ranging from 0.003 to 300 μm/s, they observed B values from -0.03 to +0.045.

Limestone and dolomite have been studied by SE and WT. In these studies, B values of opposite sign were reported; although, in SE, a sapphire disk was dragged across the rock face.

What remain are various studies in which granite and quartz were deformed under a range of conditions. At present, a comparison of these data sets provides the most insight into the factors that control the velocity dependence of the steady-state coefficient of friction. As shown in Figure 2, these granite and quartz experiments cover the entire

range of both normal stress and observed values of B. For the remainder of this paper we will concentrate on these experiments and investigate why there is so little apparent consistency in these measurements.

Variations in B due to test geometry—In many cases individual data sets plotted in Figure 2 are more self-consistent that they are consistent with results of other studies. This fact suggests the possibility of a systematic bias being incorporated into the measurements. The question then arises as to whether this bias is due to sample differences, or differences in test geometry or other test conditions. If we look only at the triaxial granite and quartz data, we find a high degree of consistency. (*Teufel and Logan's* 1978 data should not be included, since in those experiments thermal dye, which they demonstrated to have low shear strength, had been painted on the sliding surfaces. The velocity effect that they reported was of the same magnitude as the strength reduction caused by the small amount of dye on the surfaces.) The various data sets from the Byerlee lab (SB, MB, BV, LSB), as well as those of *Stesky* (1975) for granite and gabbro below 400°C (see Figure 2a), are in good agreement, even though these results cover a broad range of conditions. These conditions include room dry samples, samples with positive pore water pressure, gouge thickness ranging from 0.64 to 3.0 mm, gouge composition of granite quartz and gabbro, temperature from 22 to 400°C, sample diameter from 16 to 76 mm, sawcut samples (Byerlee) and prefractured samples (Stesky and LSBf), different jacketing techniques (polyurethane, gum rubber and thin-walled copper jackets), constant confining pressure and constant normal stress experiments, surface finishes ranging from polished to sand-blasted, and finally, a wide range of normal stress. Even with all of these variations in experimental conditions, the triaxial granite and quartz experiments give B values that generally fall in the range from -0.002 to +0.012. High temperature results from Stesky (St: 400 to 700°C) show larger B (+0.008 to +0.021). Similar experiments on sawcut samples (LSBt) and prefractured samples (LSBf) show B in the general range of -0.002 to +0.012 for temperature from 400 to 845°C. In contrast, the results of *Dieterich* (1978), *Ruina* (1980), *Tullis and Weeks* (1986), *Scholz and Engelder* (1976), and *Hungr and Morgenstern* (1984) are distinctly different. (*Dieterich and Conrad's* 1984 experiments, conducted under ultradry conditions, gave unusual results and will be discussed later.) We also note that while *Healy's* (1959) data show large scatter, they are in general agreement with the triaxial data. The range in B values reported for the various triaxial experiments is similar to the range reported by *Dieterich* (1981) for various surface roughnesses and gouge size fractions even though the values are different. Thus, with the possible exceptions of ultra-dry rock (a condition that we would not expect to find in the Earth) and rock at high temperature, the largest variations in B shown in Figure 2 for granite and quartz are associated with test geometry.

Dependence of B on total slip—If the triaxial data of Byerlee and Stesky show that B in granite and quartz is relatively insensitive to such a wide range of experimental conditions, we are forced to look elsewhere for the discrepancies with other data sets. *Dieterich* (1981) suggested that the limited displacement available in the triaxial geometry may be the problem. He presented data, obtained on his double-direct-shear press (reproduced in Figure 3a) showing how B was initially positive and then quickly became negative

with increasing displacement. *Tullis and Weeks* (1986) presented data from their rotary shear machine, showing just the opposite result (Figure 3b). Results from the Byerlee lab (Figures 3c through 3h) run under a variety of conditions at room temperature, show a general tendency for B to remain constant or become more positive with increasing displacement. This is just the opposite of the result reported by Dieterich (Figure 3a). In Dieterich's and in Tullis and Week's experiments the transient effects have passed within a few millimeters. This is well within the total slip available on the triaxial machines. Thus, run-in effects appear to be different for different test geometries. Furthermore, triaxial experiments can accommodate sufficient slip to detect initial transients in B that have been reported using other test geometries.

The apparent negative B values shown in Figure 3i for experiments conducted at elevated temperature occur at the slowest strain rates studied in the high-temperature runs. This effect is described in detail in *Lockner et al.*(1986). The remainder of the data in Figure 3i seem consistent with the lower temperature runs shown in Figure 3h.

Shimamoto (1985) has suggested a 'pre-conditioning' technique used in some triaxial experiments (*Shimamoto*, 1986, and *Shimamoto and Logan*, 1986) to shorten the displacement over which the initial strain hardening occurs. Following this procedure, a sample is first deformed at high confining pressure to quickly crush grains after which confining pressure is reduced and the desired experiment is performed. We have tested this technique on a 19 mm-diameter granite sample containing 0.64 mm of granite gouge. The sample was deformed for 2 mm at 350 MPa confining pressure after which B was measured at 250 MPa confining pressure. While shear strength was slightly higher than strength of comparable runs performed without pre-conditioning, B value was unaffected by this procedure (curve 'e' in Figure 3h).

Dependence of B on normal stress variations—Since shear strength of most geologic materials is strongly dependent on normal stress, it is possible that variations in normal stress can affect B. This argument has been used to question the validity of triaxial results since in this test geometry, both τ and σ_n typically vary during experiments. To study this effect, constant normal stress experiments have been performed on triaxial machines by *Byerlee and Vaughan* (1984) (Figure 17), *Lockner et al.* (1986) and *Morrow and Byerlee* (1985). In all cases, values of B obtained under constant normal stress conditions are in good agreement with values obtained from constant confining pressure conditions. For example, compare the constant normal stress and constant confining pressure curves in Figures 3d–3h.

It has been suggested that even momentary fluctuations in normal stress could produce strength transients that require significant displacements to dissipate, in much the same way that velocity-induced stress transients dissipate. A test of this assertion, conducted on a triaxial machine, is presented in Appendix I. The results of this test can be summarized as follows: (1) While transient shear strength effects are observed following changes in normal stress, these transients are in large part due to sliding-rate variations caused by the compliance of the loading system. Any purely normal stress induced transients must be small. In any case, these transients are found to decay over short displacements and will not affect measurements of B. (2) In geologic materials, the coefficient of friction is normal stress-dependent. This phenomenon is observed in our experiments and will have a small

effect on measurements of B taken at constant confining pressure. Values of B, measured at constant confining pressure in our experiments, should be multiplied by approximately 1.1. Thus, negative B would become more negative and positive B would become more positive. (3) All pressures are adjusted once a second in our experiments. This response time is more than adequate to maintain good control of pressures (commonly 0.1 percent) in these slowly varying experiments. Thus, in the case of the triaxial geometry, normal stress variations have little effect on the measurement of B.

Dependence of B on slip rate—As a matter of convenience, B is often assumed to be independent of the magnitude of the sliding rate. While this approximation holds for small variations in velocity, it cannot be extended to a broad range of velocities without eventually breaking down. The basis for the form of friction law in which μ^{ss} is proportional to log V is, for the most part, empirical and provides only limited insight into the physical processes that occur. At the high slip rates (>10,000 μm/s) that occur during laboratory instabilities and earthquakes, phenomena such as localized heating, melting and pore pressure fluctuations may lead to very different fault strengths than the strengths observed during low rate (0.1–10 μm/s) laboratory experiments. If stress corrosions and diffusion processes control crack growth at low slip rates, different processes will control shear strength at high slip rates. In theoretical formulations (*Dieterich*, 1981 and *Okubo and Dieterich*, 1986), this problem has been addressed by introducing high- and low-speed 'cutoff' terms into the constitutive equations.

There is evidence in the available experimental data that indicates a dependence of B on velocity. However, much of these data show little self-consistency and agreement from one data set to another is even worse. A number of examples are plotted in Figure 4. *Dieterich* (1978) plotted μ^{ss} as a function of velocity for bare granite, suggesting that B was negative at low velocity and approached zero above about 10 μm/s. In Figure 4a, we have plotted separately the three experiments from *Dieterich* (1978), using a simple linear interpolation of the original data. Only one of the three experimental runs shows a clear correlation of B with velocity. If the three runs are averaged, however, the result would be the trend shown by Dieterich. Quarzite experiments performed on the same apparatus (*Ruina*, 1980) (Figure 4b) show just the opposite trend. We have reexamined triaxial granite data first presented in *Solberg and Byerlee* (1984) at higher confining pressures. Average B values for individual experiments in which sliding rate was cycled over 3 absolute orders of magnitude, are shown in Figures 4c and 4d. (Log V_1 + log V_2)/2 is plotted on the horizontal axis. These experiments show a tendency for B to decrease with increasing velocity. Similar results were found in experiments on granite gouge containing positive pore pressure (*Byerlee and Vaughan*, 1984 and Appendix II) (Figure 4e). Other runs from these two data sets show less dependence of B on absolute velocity. *Scholz and Engelder's* (1976) data for sapphire sliding on granite (Figure 4f) show no clear velocity dependence.

Both wet and dry welded tuff data (*Teufel*, 1981) (Figure 4g) show a clear tendency for B to become less negative with increasing velocity. *Weeks and Tullis* (1985) required B to become more positive with velocity when fitting their dolomite data (Figure 4h). *Hungr and Morgenstern* (1984) report inconsistent results for 4 : 2 and 4 : 1 mixtures of quartz sand and quartz rock flour when sheared at high speeds (Figure 4i). They do not, in fact, consider any of the velocity effects that they observe to be significant. Finally, *Shimamoto*

(1986) and *Shimamoto and Logan* (1986) report large velocity related variations in B for halite gouge sliding between sandstone sample pieces (Figure 4j).

Caution should be used in comparing the various data sets in Figure 4. Because of the different forms in which the raw data are available, a number of different averaging or interpolation schemes are used in plotting the figure. Even so, it would seem difficult at this time to synthesize the available data concerning the velocity dependence of B into a single simple model.

Dependence of B on water content and temperature—*Dieterich and Conrad* (1984) performed experiments in which the fault surfaces were pre-dried at 300°C while being flushed in an ultra-dry argon atmosphere. When sheared at room temperature, samples that would normally display B of -0.014 showed B in excess of +0.022. When only minute amounts of water vapor were allowed access to the fault, B was noticeably reduced. Since *Stesky* (1975, 1978) reported a positive correlation of B with temperature ($B \simeq +0.021$ at 700°C), it would seem possible that the positive values of B reported for granite (*e.g., Solberg and Byerlee*, 1984) were the result of low water content. This, in fact, is not the case. *Byerlee and Vaughan* (1984) performed experiments in which pore water pressure of 0.5 MPa was maintained (see Appendix II). Otherwise, these experiments were identical to runs of *Solberg and Byerlee* (1984). B values (Figures 2 and 20) are consistent with B values from *Solberg and Byerlee* (1984). While early results (*Summers et al.*, 1985) from experiments similar to Stesky's seemed to show a modest increase in B at high temperature, a more complete study (*Lockner et al.*, 1986) showed essentially no temperature dependence of B up to 845°C. The discrepancies between the high-temperature results of *Stesky* (1975) and *Lockner et al.* (1986) are not yet fully understood. At the same time, it is clear that no significant difference exists between B values measured in the low temperature, room dry and water saturated triaxial experiments of *Byerlee and Vaughan* (1984), *Lockner et al.* (1986), *Morrow and Byerlee* (1985) and *Solberg and Byerlee* (1984). Thus, unless faults are very dry (a condition unlikely to occur in the Earth) we would expect water content to have little effect on B beyond the standard effective pressure rule. If sufficient time elapses for chemical alterations to occur, the presence of water could also influence shear strength through alteration processes.

Effects of Surface Roughness and Gouge Grain Size—At low normal stress, the nature of the fault surface can have an important effect on frictional strength. If the fault surface is very smooth relative to the gouge grain size, then it is possible that the gouge layer can detach from the fault surface, resulting in localized strain at the fault-gouge interface. For rougher surfaces, gouge particles in contact with the rock are forced to move with the fault surface and strain is distributed within the gouge zone. Thus, a variety of different modes of deformation can occur at low normal stress. *Dieterich* (1981) investigated these effects at 10 MPa normal stress. He found no significant variation of B with either initial gouge grain size or thickness (0.5 to 2 mm). He did, however, find that B varied with surface roughness. For surfaces hand-lapped with 600 mesh silicon carbide abrasive (fine), B averaged -0.007 $\pm$ 0.002, while surfaces prepared with 60–90 mesh abrasive (coarse) showed an average B of -0.002. At higher normal stress, gouge particles

are more quickly comminuted and fault surfaces are more quickly damaged, making starting conditions less and less important.

Little is known of the structure of active faults at seismogenic depths. In studying exhumed faults, *Wallace and Morris* (1979) and *Robertson* (1983) found a correlation between total slip and fault width, indicating that faults continue to grow with continued displacement. Wallace and Morris reported that fault zones commonly consisted of a central zone of highly comminuted gouge bordered by zones of brecciated material and finally intact rock. These observations linked with the knowledge that faults generally exhibit complex geometric structure, suggest that laboratory studies using flat, parallel rock surfaces, may be missing important effects that contribute to fault dynamics. For example, *Moore and Byerlee* (1985) have recently reported a correlation between stable or unstable slip and the magnitude of the angle of R1 'Riedel' shears in triaxial experiments. Using granite cylinders with sawcuts inclined 30° to the sample axis and containing illite gouge, they measured the angle between Riedel shears and the sawcut surfaces. When Riedel shears developed at angles less than 12°, the samples always deformed stably while for angles of 14 to 23°, stick-slip occurred. This correlation held over a range of temperatures, pressures and sliding rates. Since Riedel shears are formed by deformation oblique to the fault surfaces, stress concentrations must occur at the points where they intersect the surface. Stress inhomogeneities of this type must eventually be destroyed as slip parallel to the rock surface occurs, releasing more elastic energy for high-angle shear zones.

Recent field measurements (*Johnston et al.*, 1986) using high sensitivity strain meters have been unable to detect near-field short-term creep seconds before a number of intermediate strength earthquakes. They claim that their results are most easily explained by an inhomogeneous failure model for which various areas of the fault plane have different stress-slip constitutive laws.

Gouge dilatancy effects—In experiments performed at constant normal stress on 76 mm diameter sawcut samples containing 3 mm of saturated quartz gouge, *Morrow and Byerlee* (1985) measured slip rate-dependent changes in the gouge void ratio. In all cases, as the slip rate was increased, the gouge became more dilatant. (Recent experiments using granite gouge show the same result.) This effect may have a direct bearing on the correlation between B and test geometry.

There are a variety of ways in which velocity-dependent gouge void ratio can affect the measurement of B. For example, when surfaces are separated by very thin layers of gouge, we can expect that the high spots on the surfaces will penetrate the gouge layer and contact the opposite surface. Thus, at faster slip rates, the gouge will dilate and cause the surfaces to move farther apart. This dilation will reduce the area of contact of the surface high spots and alter the shear strength of the fault by reducing the amount of ploughing.

Other dilatancy related effects can occur that are related to specific test geometries. For example, the double-direct-shear geometry is shown in Figure 5a. In this case, normal stress is applied horizontally and the central block is driven downward between the two outer blocks. Since the vertical load applied to the top of the central block is counterbalanced by vertical forces acting on the bottoms of the outer sample parts, some rotation of the outer sample parts must occur (*Jaeger*, 1971). *N. Cook* (personal

communication, 1986) measured this 'cocking' phenomenon directly on a double-direct-shear press and found that it could not be eliminated; although *Dieterich* (personal communication, 1986) has developed techniques for reducing it. Since the outer two sample parts are pressed down onto rigid supporting blocks, velocity-dependent changes in gouge thickness will lead to velocity-dependent cocking of the sample parts (shown schematically in Figure 5b). This type of geometric effect could result in velocity-dependent variations in shear strength and therefore contribute to the measurement of B.

Another possible velocity-dependent effect is shown schematically in the insert in Figure 5a. In this case, some additional force is required, over the force needed to shear the gouge layer, to bring material from above the leading edge, down into the shear zone. In the direct shear geometry, an increase in sliding rate, accompanied by dilation of the gouge layer will lead to an increased separation of the fault surfaces. As a result, the ploughing force, occurring at the leading edge, will be reduced. This effect will result in an apparent B value more negative than that due to the shear zone alone. This effect will also occur in the shearbox geometry as well as the biaxial geometry used by *Scholz and Engelder* (1976). In the triaxial geometry, no leading edges occur; only two trailing edges where material is leaving the high-stressed region. It is interesting to note that in Figure 2, the most negative values of B are reported by Scholz and Engelder in which they slide a hard sapphire disc across a clean granite surface. We would expect this to produce the largest edge effect because the hard sapphire is not easily rounded by the softer rock. Then, in order of increasing B, we find *Ruina's* (1980) clean quartzite, *Dieterich's* (1978) clean granite, and *Dieterich's* (1981) granite with granite gouge. If a thick layer of gouge reduces the effect of the leading edge, this is just the order of results expected if the above mechanism occurs.

In the triaxial geometry, velocity-related effects on the trailing sample edges can contribute to the velocity-dependent shear strength. If such effects occur, they would likely result in determinations of B that are too positive, although we expect that this effect is small compared to the leading edge effect. Near the leading edge stresses are elevated and will enhance anelastic process, while near the trailing edge, stresses are reduced. Inhomogeneities in the stress field in the triaxial sawcut sample geometry are well known. However, when studying velocity-dependent effects, the important question is not the stress imhomogeneity, but rather how the stress field changes at different sliding velocities. While not related to gouge dilatancy, displacement on the sawcut must be accompanied by lateral slip on the piston face as well as bending of the sample column (Figure 6). Thus, if the piston-endplug interface has velocity-dependent shear strength, such properties could affect the determination of B. Depending on whether the lubricant used resulted in positive or negative velocity dependence, this could result in over- or underestimating B on the fault surface. Additional effects such as velocity-dependent seal friction have been measured and cannot account for the differences in reported values of B. (See *Lockner et al.*, 1986 for a discussion of these measurement errors.)

In rotary shear and ring shear devices, where ring-shaped samples are deformed, velocity-dependent void ratio can also affect the shear strength. For example, if gouge is distributed unevenly over the fault surface, at different sliding rates the gouge will dilate to differing degrees, changing the distribution of normal stress and consequently

shear strength. Since, in these experiments, torque, rather than shear stress, is measured, changes in the radial distribution of shear stress can be misinterpreted. Thus, in ring shear experiments, the way that the test material is initially packed in the test apparatus can be important. If the test material is overcompacted near the inner radius of the machine, dilatancy effects will lead to higher normal stress and shear strength in this region. Also, in the rotary geometry, material near the outside of the annulus must undergo greater total strain than material near the inside. Thus, in high normal stress rotary shear experiments such as *Tullis and Weeks* (1986), one might expect the development of a thicker, more highly comminuted gouge layer near the outside of the sample. As shown in Figure 7, velocity-induced dilation of a gouge layer of nonuniform thickness could result in a change in the distribution of normal stress and consequently shear strength. This could result in a misleading change in torque.

All of these questions regarding the geometric effects of velocity-dependent void ratio should be studied in detail. The various dilatancy-related effects that we have just presented are notably subtle. At the same time, the reported velocity-dependent strength effects are also small; typically one percent or less of the nominal shear strength for a decade change in slip rate. We expect that theoretical modeling of these effects in laboratory samples will generally be unsatisfactory since the stress and strain fields involved are complex and we are dealing with a combination of elastic and anelastic processes. It would seem desirable to design and conduct experiments to measure these effects directly and thereby determine if they are significant.

Instability

A primary goal of this research has been to increase our understanding of earthquake processes. The theoretical analysis of velocity- and slip history-dependent friction laws and how they relate to fault instability is a complex subject which we will not discuss in any great detail here. However, we will present some recent laboratory results that are of interest.

In a triaxial experiment conducted at constant confining pressure, instability will occur when more potential (elastic) energy is supplied by the loading system than can be dissipated by the fault surface. This condition is shown graphically in Figure 8 in which differential stress ($\sigma_\Delta = \sigma_1 - P_c$) is plotted versus the component of fault slip that is parallel to the sample axis. In the first example, the sample deforms stably since the slope of the fault weakening curve is everywhere shallower than the slope along which the machine will unload (shown as a dashed line). In the second example, the fault becomes unstable at point a where it weakens faster than the unloading rate of the machine and does not come to rest until point b where the excess elastic energy has been dissipated. Note that this stability criterion places no restrictions on the sign or magnitude of B. Rather, instability occurs when the maximum rate of fault weakening ($\simeq \sigma_d/d_r$ in Figure 8) exceeds the machine unloading rate. This concept is discussed by *Dieterich* (1978). For triaxial granite experiments, σ_d generally increases with confining pressure, while d_r seems to have little pressure dependence. For example, *Dieterich* (1981) reported d_r of ranging from 100–200 μm for 1 mm thick granite gouge at σ_n 10 MPa while triaxial granite data at 300 MPa confining pressure (Figure 18) show similar values. Thus displacement-weakening should

increase with increasing confining pressure. Since, for a given test apparatus, machine stiffness has little pressure dependence, deformation should become more unstable at higher confining pressure *Dieterich* (1978). This effect would explain the transition from stable to unstable deformation accompanying an increase in normal stress in some experiments (*e.g., Stesky*, 1975, 1978). A tendency for d_r to increase with temperature (*Lockner et al.*, 1986) would similarly lead to increased stability with temperature. As the displacement weakening rate approaches the machine unloading rate, an abrupt transition from stable to unstable slip will not always occur. Instead, the instantaneous velocity strengthening effect (eq. 5) will tend to stablize the fault and lead to a transition region characterized by accelerated creep and oscillatory creep as described by *Dieterich* (1981) and *Tullis and Weeks* (1986).

For the purposes of this discussion, the machine stiffness k is divided into two parts: the stiffness of the sample column above the point where displacement is controlled (k_a) and the stiffness of the ram and sample column below the displacement control point (k_r) (see Figure 9 and Appendix I). For deformation which is under servo control (quasi-static), effects of the ram stiffness are eliminated by the control system, and the critical unloading rate is given by k_a/A where A is cross-sectional area of the sample. Once an instability begins and slip rate is faster than the servo control system can respond, both the ram and the sample column contribute to the unloading rate. This dynamic unloading rate is $1/A(k_a k_r/(k_a + k_r))$

Lockner et al.(1986) have recently conducted a series of triaxial experiments at 250 MPa confining pressure, using 30°sawcut granite samples and 0.64-mm-thick granite gouge layers. Experiments were run between 22 and 845°C. B values, along with those reported by *Stesky* (1975), are summarized in Figure 10 and Table 2 and show B to be slightly positive and nearly independent of temperature. Representative experiments are plotted in Figure 11 as differential stress (corrected for sawcut contact area) versus $L_a \equiv z - \sigma_1 A/k_a$ where z is axial shortening as measured at the displacement control point. L_a represents the computed slip on the sawcut resolved parallel the sample axis (essentially correcting for the elastic shortening of the sample column). Figure 12 provides a comparison of the deformation rate imposed at the displacement control point and the resulting slip rate on the sawcut. The character of the velocity-induced stress transients shown in Figure 11 clearly changes with temperature. The distance d_r overwhich transients decay is greater at the highest temperature. At the highest and lowest temperatures, stress transients are dissipated in a stable, monotonic (overdamped) decay mode. At intermediate temperatures, however, deformation is unstable; both oscillatory decay and stick-slip occur. Oscillatory decay is transient stress decay which overshoots the steady-state stress level for at least one-half cycle, while stress changes are slow enough that the displacement remains under servo control at all times. (Response of the servo control system is down 3dB at approximately 1 Hz.) In all but one case, stick-slip occurred during displacement-weakening transients following imposed velocity step increases. Stress drops were always small (5–20 MPa) and were, in some cases, audible. We define stick-slip events, in this section, as any stress drops that occur too fast to remain under servo control. Thus, for stable monotonic and oscillatory decay events the fault 'sees' the quasi-static machine stiffness (determined in these experiments to be k_a/A=580 MPa/mm). Stick-slip events

will see machine stiffness as low as the dynamic stiffness (480 MPa/mm for this machine and sample size).

The transition from stable to unstable deformation at different temperatures must reflect a change in the material properties of the fault since in all experiments, the machine and sample column assemblies were the same. It is also interesting that this transition in deformation mode occurred even though there was little associated variation in B. To further examine this effect, we studied the transient stress decays following imposed velocity step increases for all events at 2.5 mm or more total axial shortening. The maximum rate of weakening of differential stress was determined for each event. This parameter is plotted as a function of temperature in Figure 13 along with the quasi-static and dynamic machine stiffnesses. Symbols separate events according to decay type and deformation rate. Slower strain rates tend to have faster maximum stress weakening rates. The stable, monotonic decays occurred in two temperature ranges: from room temperature to 150°C and from 550°to 850°C. In between, oscillatory decays and stick-slip occurred. Stress weakening rates of the monotonic decay events were generally less steep than those of the oscillatory and stick-slip events. This observation is consistent with the stability criterion discussed above. The fact that three stick-slip events have shallow slopes (-370 to -400 MPa/mm) is probably the result of an inadequate sampling rate. Since stress and displacement are sampled only once a second, the true slopes of these fast events cannot be accurately resolved. The temperature range over which stick-slip events occur is, however, of interest. The unstable deformation occurring at intermediate temperatures is apparently controlled more by a minimum in d_r than by any change in σ_d (related to b in *Rice and Gu*, 1983) or B.

CONCLUSIONS

In this paper, we have reviewed the available laboratory data on the velocity dependence of the steady-state coefficient of friction in geologic materials. The velocity dependence of μ^{ss} has been expressed by a parameter B which represents the change in μ^{ss} for a decade change in sliding rate. Reported values of B for granite and quartz (Figure 2) generally fall in the range -0.03 to $+0.03$. Although, at normal stresses representative of seismogenic depths, a range of B from -0.025 to $+0.010$ seems more appropriate. In experiments performed on a single machine, variations in surface roughness, gouge particle size, sawcut samples with gouge vs. prefractured samples, normal stress and absolute sliding rate can alter B by as much as 0.01. When adsorbed water is removed from the fault zone, B can be altered 3 to 4 times this amount. In one study, heating to 700°C increased B by 0.02 whereas in a second study, heating to 845°C had little effect. Finally, measurements of B for similar material deformed in different test geometries can vary by 0.01 or more. We consider this last fact to be of some significance. At the present time, we cannot rule out the possibility that most of the variation in B that has been reported for geological materials is due to subtle effects of test geometry and not to material properties of the fault. Most materials in bulk (*McClintock and Argon*, 1966) show strengthening with increased strain rate, although the presence of the rigid boundaries on faults can have a significant effect. Since we have only a limited understanding of the physical processes that control the velocity-dependence of frictional strength, we should be cautious in applying presently

available laboratory data to earthquake field problems. If machine-related geometric effects contribute significantly to the apparent velocity dependence observed in laboratory experiments, similar geometric effects, occurring naturally on faults, may also contribute to earthquake mechanisms.

REFERENCES

Boatwright, J., The effect of rupture complexity on estimates of source size, *J. Geophys. Res.*, **89**, 1132–1146, 1984.

Bowden, F. P. and Tabor, D., *The Friction and Lubrication of Solids*, Part II, Oxford University Press, London, 544 p., 1964.

Byerlee, J. D., Frictional characteristics of granite under high confining pressures, *J. Geophys. Res.*, **72**, 3639–3648, 1967.

Byerlee, J. D., Brittle-ductile transition in rocks, *J. Geophys. Res.*, **73**, 4741–4750, 1968.

Byerlee, J. D., The mechanics of stick-slip, *Tectonophysics*, **9**, 475–486, 1970.

Byerlee, J. D., Friction of rocks, *Pure and Appl. Geophys.*, **116**, 615–626, 1978.

Byerlee, J. D. and Vaughan, P., Dependence of friction on slip velocity in water saturated granite with added gouge, *EOS, Trans. Amer. Geophys. Union*, **65**, 1078, 1984.

Dieterich, J. H., Time-dependent friction and the mechanics of stick-slip, *Pure and Appl. Geophys.*, **116**, 790–806, 1978.

Dieterich, J. H., Experimental and model study of fault constitutive properties, in *Solid Earth Geophysics and Geomechanics, Appl. Mech. Div.*, **42**, A.S.M.E., ed. S. Nemat-Nasser, 21–29, 1980.

Dieterich, J. H., Constitutive properties of faults with simulated gouge, in *Mechanical Behavior of Crustal Rocks, Am. Geophys. Union Monograph*, 24, 103–120, 1981.

Dieterich, J. H. and Conrad, G., Effect of humidity on time- and velocity-dependent friction in rocks, *J. Geophys. Res.*, **89**, 4196–4202, 1984.

Engelder, J. T., Logan, J. M. and Handin, J., The sliding characteristics of sandstone of quartz fault gouge, *Pure Appl. Geophys.*, **113**, 69–86, 1975.

Healy, K. A., The dependence of dilation in sand on rate of shear strain, Ph.D. Thesis, Massachusetts Inst. of Tech., 1959.

Hungr, O. and Morgenstern, N. R., High velocity ring shear tests on sand, *Geotechnique* **34**, 415–421, 1984.

Jaeger, J. C., Friction of rocks and stability of rock slopes, *Geotechnique*, **21**, 97–134, 1971.

Johnston, M. J. S., Linde, A. T., Gladwin, M. T., Borcherdt, R. D., Fault Failure with Moderate Earthquakes, *Tectonophysics*, in press.

Kanamori, H. and Stewart, G. S., Seismological aspects of the Guatemala earthquake of February 4, 1976, *J. Geophys. Res.*, **83**, 3427–3434, 1978.

King, G. C. P., The geometry of the initiation and termination of earthquake rupture and the evolution of morphology and geological structures, submitted to *5th Ewing Symposium, Earthquake Source Mechanisms*, AGU Monograph, 1986.

King, G. and Nabelek, J., Role of fault bends in the initiation and termination of earthquake rupture, *Science,* **228**, 984–987, 1985.

Lockner, D. A., Summers, R., and Byerlee, J. D., Effects of temperature and sliding rate on frictional strength of granite, *Pure and Appl. Geophys.*, in review.

McClintock, F. A. and Argon, A. S., Mechanical behavior of materials, Addison-Wesley, 1966.

Moore, D. E. and Byerlee, J. D., Deformation textures developed in heated fault gouge, *EOS, Trans. Amer. Geophys. Union,* **66**, 1100, 1985.

Morrow, C. and Byerlee, J. D., A physical explanation for transient stress behavior during shearing of fault gouge at variable strain rates *EOS, Trans. Amer. Geophys. Union,* **66**, 1100, 1985.

Okubo, P. G. and Dieterich, J. H., State variable fault constitutive relations for dynamic slip, submitted to *5th Ewing Symposium, Earthquake Source Mechanisms*, AGU Monograph, 1986.

Rice, J. R., Constitutive relations for fault slip and earthquake instabilities, *Pure and Appl. Geophys.,* **121**, 443–475, 1983.

Rice, J. R. and Gu, J.-C., Earthquake aftereffects and triggered seismic phenomena, *Pure and Appl. Geophys.,* **121**, 187–219, 1983.

Rice, J. R. and Ruina, A. L., Stability of steady frictional slipping, Trans. ASME, *J. Appl. Mech.,* **50**, 343–349, 1983.

Robertson, E. C., Relationship of fault displacement to gouge and breccia thickness, *Trans. A.I.M.E.,* **35**, 1426–1432, 1983.

Ruina, A. L., Friction laws and instabilities: A quasistatic analysis of some dry frictional behavior, Ph.D. Thesis, Brown University, 1980.

Ruina, A. L., Slip instability and state variable friction laws, *J. Geophys. Res.,* **88**, 10359–10370, 1983.

Schneider, H., The time-dependence of friction of rock joints, *Bull. Int. Assoc. Engin. Geol.,* **16**, 235–239, 1977.

Scholz, C. H. and Aviles, C. A., The fractal geometry of faults and faulting, submitted to *5th Ewing Symposium, Earthquake Source Mechanisms,* AGU Monograph, 1986.

Scholz, C. H. and Engelder, J. T., The role of asperity indentations and ploughing in rock friction, I. Asperity creep and stick slip, *Int. J. Rock Mech. Mining Sci. Geomech. Abstr.,* **13**, 149–154, 1976.

Segall, P. and Pollard, D. D., Mechanics of discontinuous faults, *J. Geophys. Res.,* **85**, 4337–4350, 1980.

Shimamoto, T., Confining pressure reduction experiments: a new method for measuring frictional strength over a wide range of normal stress, *Int. J. Rock Mech. Min. Sci. and Geomech. Abstr.,* **22**, 227–236, 1985.

Shimamoto, T., Transition between frictional slip and ductile flow for halite shear zones at room temperature, *Science,* **231**, 711–714, 1986.

Shimamoto, T. and Logan, J. M., Velocity-dependent behaviors of simulated halite shear zones: An analog for silicates, submitted to *5th Maurice Ewing Symposium, Earthquake Source Mechanics*, AGU Monograph, 1986.

Sibson, R. H., Rupture interactions with fault jogs, submitted to *5th Ewing Symposium, Earthquake Source Mechanisms,* AGU Monograph, 1986.

Skempton, A. W., Residual strength of clays in landslides, folded strata and the laboratory, *Geotechnique,* **35**, 3–18, 1985.

Solberg, P. and Byerlee, J. D., A note on the rate sensitivity of frictional sliding of Westerly granite, *J. Geophys. Res.,* **89**, 4203–4205, 1984.

Stesky, R. M., Mechanisms of high-temperature frictional sliding in Westerly granite, *Can. J. Earth Sci.,* **15**, 361–375, 1978.

Stesky, R. M., The mechanical behavior of faulted rock at high temperature and pressure, Ph.D. Thesis, Massachusetts Inst. of Tech., 1975.

Summers, R., Lockner, D. A., and Byerlee, J. D., Temperature and velocity dependence of friction in granite, *EOS, Trans. Amer. Geophys. Union,* **66**, 1100, 1985.

Teufel, L. W., Frictional properties of jointed welded tuff, *SAND* 81-0212, *Sandia National Laboratories*, 1981.

Teufel, L. W. and Logan, J. M., Effect of displacement rate on the real area of contact and temperatures generated during frictional sliding of Tennessee sandstone, *Pure and Appl. Geophys.,* **116**, 840–865, 1978.

Tse, S. T. and Rice, J. R., Crustal earthquake instability in relation to the depth variation of frictional slip properties, *J. Geophys. Res.*, in press.

Tullis, T. E. and Weeks, J. D., Constitutive behavior and stability of frictional sliding of granite, *Pure and Appl. Geophys.*, in press.

Tullis, T. E., Weeks, J. D. and Blanpied, M., Constitutive behavior and stability of frictional sliding in granite, submitted to *5th Ewing Symposium, Earthquake Source Mechanisms,* AGU Monograph, 1986.

Wallace, R. E. and Morris, H. T., in Proc. Conf. VIII, Analysis of actual fault zones in bedrock, *U.S. Geol. Survey Open File Report 79–1239*, 79–100, 1979.

Weeks, J. and Tullis, T., Frictional behavior of dolomite: A variation in constitutive behavior, *J. Geophys. Res.,* 90, 7821–7826, 1985.

Table 1. Measurements of B

		Data Points	Gouge Material	Test Surface	Machine	Comments
BV	Byerlee and Vaughan (1984); Appendix II	42	granite	granite	triaxial	With pore pressure
D	Dieterich (1978)	> 32	—	granite	direct shear	
DC	Dieterich and Conrad (1984)	7	—	granite/ quartzite	direct shear	Ultra-dry
Dg	Dieterich (1981)	29	granite	granite	direct shear	
He	Healy (1959)	15	sand: quartz/ quartzite & feldspar		ring shear	
HM	Hungr and Morgenstern (1984)	48	quartz		ring shear	
LSB	Lockner, Summers and Byerlee (1986)	13	granite	granite	triaxial	Up to 400°C
LSBf	Lockner, Summers and Byerlee (1986) (high temp.)	9	granite	granite	triaxial	Pre-fractured 676°C
LSBt	Lockner, Summers and Byerlee (1986) (high temp.)	12	granite	granite	triaxial	Sawcut, 400–845°C
MB	Morrow and Byerlee (1985)	19	quartz	granite	triaxial	With pore pressure
R	Ruina (1980)	23	—	quartzite	direct shear	

Table 1. Measurements of B
(continued)

		Data Points	Gouge Material	Test Surface	Machine	Comments
S	Stesky (1975); granite	7	granite	granite	triaxial	Pre-fractured, 300–400°C
SB	Solberg and Byerlee (1984)	80	granite	granite	triaxial	
Sc	Schneider (1977)	~210	clay		shear box	
SE	Scholz and Engelder (1976)	39	—	granite, limestone, dunite	biaxial	On sapphire
Sg	Stesky (1975); gabbro	4	gabbro	gabbro	triaxial	pre-fractured, 300–400°C
Sh	Shimamoto (1985)	4	chlorite	sandstone	triaxial	
Sk	Skempton (1985)	112	clay		ring shear	
St	Stesky (1975) (high temp.)	11	granite	granite	triaxial	Pre-fractured, 400–700°C
T	Teufel (1981)	29	—	welded tuff	ring shear	Wet and dry
TL	Teufel and Logan (1978)	4	—	sandstone	triaxial	Thermal dye on surface
TW	Tullis and Weeks (in press)	~45	—	granite	rotary shear	
WT	Weeks and Tullis (1985)	5	—	dolomite	rotary shear	

Table 2. Experimental Conditions in Figure 10

Figure Label	Temp °C	Number of Measurements	Sample Diameter mm	Bore Hole	Graphite Sleeve	Cu Sleeve Thickness mm	Comments
diamonds	300–700	18	16	no	yes	0.32	Pre-fractured samples
circles	22–845	21	19.05	yes	no	0.25	Sawcut samples with gouge (high-confidence data from Figure 21 and Lockner *et al.*, 1986)
a	22	2	19.05	yes	no	0.25	Sawcut sample with gouge, 'pre-conditioned' for 2 mm at P_c = 350 MPa, run at P_c = 250 MPa
b	696	3	19.05	yes	no	0.25	Sawcut sample with gouge, 0.5 MPa pore pressure
c	321	3	15.88	no	yes	0.25	Sawcut sample with gouge
	696	5	"	"	"	"	" "
d	696	7	15.88	yes	yes	0.51	Sawcut sample with gouge, pre-dried
e	676	5	15.88	no	yes	0.51	Pre-fractured sample, fracture angle = 25°
f	676	4	15.88	no	yes	0.51	Pre-fractured sample, fracture angle = 21°, pre-saturated

FIGURE CAPTIONS

Fig. 1. Common response of fault during laboratory test in which sliding rate is abruptly increased from V_1 to V_2. (a) Experimental data from decade velocity increase at 250 MPa confining pressure. (b) Schematic representation showing parameters used in this report. In general, μ goes through a transient peak before decaying to μ^{ss}. Parameter d_r, as defined here, is similar, but not identical to d_r as used by *Dieterich* (1981).

Fig. 2. Summary of available data on rate sensitivity of steady-state coefficient of friction in geologic materials (see Table 1 for details of the various data sets). Horizontal error bars give total normal stress range; vertical error bars represent approximately 1 standard deviation in B. Dg represents range of values for a variety of surface roughnesses and gouge grain sizes. In some data sets (*e.g.*, BV, D, SB, and T) B correlates with absolute sliding rate. This effect is pronounced in *Shimamoto* (1986) and is not plotted here due to the complexity of the data set (see Figure 4j). Figure 2a shows high normal stress data in greater detail.

Fig. 3. Evolution of B with total displacement. (a) From *Dieterich* (1981); 1 mm granite gouge between granite surfaces at 10 MPa normal stress on double-direct-shear press. (b) From *Tullis and Weeks* (1986); rough granite surfaces, no initial gouge layer, rotary shear machine, 80 MPa normal stress. (c) and (d) data used in *Solberg and Byerlee* (1984); 1 mm granite gouge between granite surfaces, triaxial press. (e) and (f) from *Byerlee and Vaughan* (1984) (see Appendix II); 1 mm granite gouge between granite surfaces with 0.5 MPa pore pressure; triaxial press. (g) data from *Morrow and Byerlee* (1985); 3 mm quartz gouge between granite surfaces with 0.5 MPa pore pressure; triaxial press. Cyclic variations in plots c–f are primarily due to sliding rate during measurements. Faster rates tend to give lower B values. (h) and (i) data from *Lockner et al.* (1986); 0.64 mm granite gouge between granite surfaces at various temperatures. Curve 'e' in Figure 3h is data from 'pre-conditioned' run.

Fig. 4. Plots of velocity dependence of B. (a) Interpolated granite data from *Dieterich* (1978), no gouge, double-direct-shear press 2 MPa normal stress; (b) quartzite data from *Ruina* (1980), no gouge, double-direct-shear press, 3 MPa normal stress; (c) and (d) granite data from *Solberg and Byerlee* (1984), 1 mm granite gouge, triaxial press; (e) granite data from *Byerlee and Vaughan* (1984) (see Appendix II), 1 mm granite gouge, 0.5 MPa pore pressure, triaxial press; (f) sapphire on granite data from *Scholz and Engelder* (1976), no gouge, biaxial press; (g) welded tuff data from *Teufel* (1981), no gouge, wet and dry, ring shear press; (h) results of computer simulation of dolomite data from *Weeks and Tullis* (1985), no gouge, 80 MPa normal stress, rotary shear press; (i) quartz data from *Hungr and Morgenstern* (1984), 4 : 2 and 4 : 1 mixtures of quartz sand and

crushed quartz rock flour, high-speed low normal stress ring shear tests; (j) halite on sandstone data from *Shimamoto* (1986), triaxial press.

Fig. 5. Schematic diagram of double-direct-shear press geometry. (a) Insert shows geometry that can lead to leading-edge ploughing stress (not drawn to scale). Velocity-dependent gouge dilatancy can alter leading-edge geometry. (b) Since outer sample parts are pinned to lower support pieces by application of vertical load (shim will act as a pivot point), velocity-dependent gouge dilatancy can lead to cocking of the sample assembly at different slip rates. (Effects are not drawn to scale.)

Fig. 6. Schematic diagram of triaxial press geometry. Slip on fault surface requires lateral slip of sample column (generally on piston-end plug interface). Velocity-dependent friction on this surface can complicate measurements of B on sawcut. This geometry contain only trailing edges where material leaves high stress regions. Effects of jacketing and seal friction are discussed in *Lockner et al.*(1986).

Fig. 7. Schematic diagram of rotary shear press showing one possible effect of velocity-dependent gouge dilatancy. At different slip rates, the radial distribution of normal stress, and consequently shear strength, will change. Since torque is measured and then used to infer average shear stress, this and related effects can lead to systematic errors in measuring shear stress.

Fig. 8. Examples of a) stable and b) unstable stress/displacement histories. Slope of dashed line represents unloading rate of the test system. When fault weakens at a faster rate than the unloading rate of the test system (point 'a'), excess elastic energy leads to accelerating slip and instability. Fault eventually comes to rest at point 'b' where excess energy has been dissipated. For stable slip, maximum rate of fault weakening is approximately σ_d/d_r.

Fig. 9. (a) Schematic drawing of axial load components in triaxial apparatus. (b) Equivalent elements of machine stiffness, separated by point where displacement is servo controlled. Servo control has the effect of making $k_r \rightarrow \infty$.

Fig. 10. B versus temperature plot. Diamonds are *Stesky's* (1975) granite data; circles are from 19.05 mm-diameter runs of *Lockner et al.*(1986). Data bars represent results from additional experiments in *Lockner et al.*(1986) (see Table 2).

Fig. 11. Detailed stress-displacement curves of selected runs in *Lockner et al.*(1986) showing change in deformation mode at various temperatures. Horizontal axis is computed displacement on sawcut (correcting for machine stiffness and inclination of sawcut to sample axis).

Fig. 12. Example of computed slip rate on sawcut (correcting for machine stiffness and inclination of sawcut to sample axis) that results from step changes in

velocity at the displacement control point. $\mathrm{Log}_{10} V_{sawcut}$ is computed every second using a running window. This window is 4s at fastest slip rate; 40s at intermediate slip rate and 400s at slowest slip rate.

Fig. 13. Plot of maximum rate of weakening of sawcut versus temperature for experiments in *Lockner et al.*(1986) (see text). Quasi-static and dynamic machine stiffnesses for the test apparatus and sample size used in these experiments are plotted.

Fig. 14. Test of normal stress dependence of μ (see Appendix I). Horizontal axis is computed slip on sawcut; correcting for machine stiffness and inclination of sawcut to sample axis. 1 mm granite gouge between granite surfaces. Plotted from top to bottom are: μ, σ_n, $\log_{10}$ (slip rate on sawcut) and $\log_{10}$ (axial shortening rate at control point). Velocities are averaged over 50 s windows; sampling rate is 1/s. Due to compliance of sample column, changes in σ_n produce slip rate transients on the sawcut even though axial shortening rate (at displacement control point) is constant. Strain rates in legend correspond to axial shortening rates of 4.8×10^{-3}, 4.8×10^{-4} and 4.8×10^{-5} mm/s.

Fig. 15. Sample assembly. Pore water pressure is applied through the hole in the upper end plug which connects directly to a blind hole in the upper part of the sample.

Fig. 16. Representative plot of friction coefficient (μ) and normal stress (σ_n) on the sawcut surface versus axial displacement. Axial shortening rates are given in μm/s.

Fig. 17. Coefficient of friction (μ) and normal stress (σ_n) plotted vs. axial displacement for an experiment on dry Westerly Granite gouge in which the confining pressure was servo-controlled to maintain constant normal stress.

Fig. 18. Detailed portions of μ vs. axial displacement for two experiments.

Fig. 19. Friction coefficient (μ) vs. z (axial displacement or shortening of the sample) for run VF4. Stick-slip events occurred independently of changes in imposed slip rate. Stable sliding occurred in the experiment but, after 7 mm of axial displacement, stick-slip occurred exclusively.

Fig. 20. Plot of slip rate sensitivity, B, against normal stress for four water-saturated experiments at two confining pressures. The small numbers indicate the number of data points at places where several occur.

APPENDIX I—Dependence of B on Normal Stress

In the past, nearly all triaxial experiments have been performed at constant confining pressure. This was true for Stesky's experiments as well as the majority of the various Byerlee experiments. Because the sliding surface is inclined to the sample axis, both shear (τ) and normal (σ_n) stress on the fault are functions of axial stress (σ_1). For a sawcut inclined 30° to the sample axis we have

$$\tau = \frac{\sigma_\Delta}{2} \sin(2 \times 30°) \simeq 0.433\, \sigma_\Delta \tag{6a}$$

and

$$\sigma_n = P_c + \frac{\sigma_\Delta}{4} \tag{6b}$$

where P_c is confining pressure and σ_Δ is differential stress $= \sigma_1 - P_c$. Thus, in a triaxial experiment at constant confining pressure, both τ and σ_n increase with increasing axial stress. If B depends on normal stress, then the changes in normal stress that occur in constant P_c triaxial experiments may affect estimates of B. *Solberg and Byerlee* (1984) studied this effect. They found a small positive correlation between B and σ_n : $\partial B/\partial(\log_{10} \sigma_n) = 0.0032$. In constant confining pressure experiments, normal stress would typically rise by about 10 percent over the entire range of measurements. Thus, this effect should not contribute any significant error to the determination of B. In fact, a comparison of constant-P_c and constant-σ_n experiments in Figures 2d–2g confirms this expectation.

To conduct controlled normal stress experiments, σ_n is computed once a second using (6b) and then confining pressure is adjusted by an appropriate amount to correct deviations in σ_n. For the slow stress variations that occur at the sliding rates used (< 5 μm/s), a one second control loop is sufficient to maintain normal stress to within 0.2 MPa for experiments run at 50 MPa or more. Following stick-slip events, however, a few seconds are generally required to bring normal stress back to the desired value.

It is possible that variations in normal stress can produce shear strength transients that decay with displacement in much the same manner that velocity-induced transients decay. If such normal stress-induced transients occur, they could affect the constant-P_c measurements performed on triaxial machines. To investigate this phenomenon, we have conducted an experiment in which a 1 mm thick room dry Westerly granite gouge layer was deformed between 76.2 mm diameter Westerly sample halves. In this experiment, normal stress was altered in steps of up to 5 MPa, and resulting transients in coefficient of friction were recorded. These normal stress fluctuations are much larger than the fluctuations occurring in any of our standard triaxial experiments conducted at either constant normal stress or constant confining pressure. We will discuss the experiment and results (shown in Figure 14) in some detail since proper interpretation of the data requires an understanding of the operation of the triaxial machine.

In all of our experiments, displacement of the steel piston, used to deform the sample, is measured at a point outside of the pressure vessel. Thus the sample assembly and piston all contribute to an elastic axial stress loading constant, measured on this machine

to be $k_a/A = 160$ MPa/mm. Thus, if the piston were advanced 1 mm as measured at the displacement control point, and no slip occurred on the sawcut, the axial stress would increase by 160 MPa. For a constant normal stress experiment, this results in a shear stress stiffness of approximately $k_s/A \sim 90$ MPa/mm. To aid in explaining the experiment shown in Figure 14, the displacement plotted on the horizontal axis is not the displacement (z) measured at the displacement control point. Instead, we have plotted the computed displacement on the sawcut $L \equiv z - \sigma_1 A/k_a)\cos(30°)$. Here we have corrected for both elastic shortening of the sample column and the fact that the sawcut is inclined to the sample axis.

The piston was advanced, as measured at the displacement control point, at 2 μm/s until A, then at 0.2 μm/s until B and finally 1 μm/s for the remainder of the plot. From the velocity step data around A and B in Figure 14 we conclude that at 50 MPa normal stress, in this experiment $B = 0 \pm 0.0005$. Small sudden fluctuations in $\mu < 0.0003$ are sampling noise, while larger changes (at A and B, for example) are real shear stress fluctuations. When normal stress was suddenly dropped, as at E and F, stick-slip events occurred, characterized by audible stress drops at 2 to 5 MPa.

Starting at C in Figure 14 normal stress was altered by adjusting the confining pressure. Due to the compliance of the sample column, when normal stress was increased, as at C, shear stress momentarily dropped below the shear strength of the fault and sliding on the fault surface ceased. As the piston continued to advance, shear stress eventually reached the shear strength and sliding on the sawcut resumed. Sliding rate on the sawcut, $\log_{10}(dL/dt)$, averaged over a 50 s time interval, is plotted at the bottom in Figure 14. This shows the sudden drop in sliding rate on the sawcut when normal stress is increased. When normal stress is decreased, as at D, the compliance of the sample column results in a slip rate on the sawcut that is momentarily faster than the rate imposed at the displacement control point. Apparently, much, if not all, of the transient response of μ following normal stress steps, is a result of these slip rate transients. Note the similarity to the purely slip rate induced transient occurring at A.

Steady-state coefficient of friction μ^{ss} is clearly normal stress dependent (*e.g.*, $\Delta\mu^{ss} \sim$ 0.0055 between E and F in Figure 14). This is true, in general, for geological materials. At normal stress up to 200 MPa, τ vs. σ_n plots for rocks are, in general, concave-downward (*Byerlee*, 1968). Above 200 MPa, most common rocks (*Byerlee*, 1978) and Westerly granite in particular (*Byerlee*, 1967) obey the shear strength relation (1b) or, in terms of coefficient of friction, relation (2b). Differentiation of (2b) gives

$$\Delta\mu \simeq -50\frac{\Delta\sigma_n}{\sigma_n^2}\ [\text{MPa}] \tag{7}$$

As a result, we expect μ^{ss} to decrease with increasing normal stress as observed in Figure 14. The effect that this normal stress dependence has on constant-P_c experiments is that the magnitude of B will be underestimated. From (7) we conclude that at $P_c = 250$ MPa, all values of B should be multiplied by approximately 1.1, making positive B more positive and negative B more negative. To help clarify this effect, we use the following example. Let us assume that at $V = 0.1$ μm/s, $\mu^{ss}_{0.1} = 0.700$. Let us further assume that when the sliding rate is increased to 1 μm/s, $\mu^{ss}_{1.0} = 0.710$. From (3) we estimate $B = 0.01$.

From (6), however, we know that σ_n has increased from 419.6 to 423.7 MPa. From (7), the change in normal stress should have reduced μ^{ss} by 0.0012. Thus, $\Delta\mu^{ss}$ in (3), and therefore B, should really be 0.0112. The normal stress dependence in Figure 14 at 50 MPa along with results of a similar experiment at $\sigma_n = 250$ MPa indicate that the magnitude of B should be increased by approximately 10 percent for constant-P_c triaxial experiments over this entire range of normal stress.

Recent results of *Morrow and Byerlee* (1985) indicate that velocity-related strength transients are closely related to the degree of gouge compaction and dilation. Because changes in normal stress (especially increases in normal stress) also affect gouge compaction, we expect normal stress-induced strength transients to occur, as well. What we have attempted to demonstrate in this section is that normal stress-induced strength transients will have little effect on the determination of the steady-state parameter B.

APPENDIX II—Frictional Strength of Water-Saturated Westerly Granite

Dieterich and Conrad (1984) showed that a dramatic shift from negative to positive B occurred in granite and quartzite when the fault deformed under ultry-dry conditions. On this basis, it has been suggested that the positive B reported for room dry granite by *Solberg and Byerlee* (1984) was the result of over-drying the samples. In this appendix, we present data, first discussed by *Byerlee and Vaughan* (1984), to test this hypothesis.

Experimental Method

The experimental procedures were essentially the same as those described by *Solberg and Byerlee* (1984) with the addition of a 0.5 MPa pore water pressure. The samples were cylinders of granite 63.5 mm long, 25.4 mm in diameter with sawcuts inclined 30° to the sample axis. Both ends of each sample were surface ground with an 80 grit wheel. The sawcut itself was not surface ground except for the VF7 and VF9 samples. A layer of crushed Westerly granite (size fraction 150 to 200 mesh, 1 mm thick) was spread along the sawcut. A blind hole, 2 mm in diameter, was drilled in one piece of each sample to a depth approximately 1 mm from the sawcut (Figure 15). This hole permitted pore water access to a region very close to the fault, thus insuring that pore water could move in and out of the fault zone. The samples were saturated with deionized water prior to assembly. They were jacketed with 3 mm thick polyurethane tubes which extended up to the top endplug in order to isolate the pore pressure and confining pressure systems (Figure 15).

A fluid confining medium, either kerosene or silicon oil, applied constant confining pressure to the samples throughout each experiment. Confining pressure was maintained constant by servo control at either 30 or 300 MPa. The samples were shortened in compression at axial shortening rates of 0.00635 to 6.35 μm/s. Two experiments were conducted at each of the two confining pressures. One, in which slip rates were varied in the order $(6.35\times)10^{-3}$ to 10^{-2} to 10^{-1} to 10^{0} to 10^{-3} μm/sec and the other had order $(6.35\times)10^{0}$ to 10^{-1} to 10^{-2} to 10^{-3} to 10^{0} μm/sec. The displacement on the sawcut per step was 0.5 mm. Total axial displacement was 10 mm. Data consisting of axial load, axial displacement and confining pressure were recorded every 2 seconds during the experiment. The shear and normal stresses on the sawcut were calculated from these values.

Observations

The friction-displacement curves for experiments with stable sliding were similar to those observed by *Solberg and Byerlee* (1984) for dried samples. They consisted of an initial linear segment representing elastic strain in the sample column and a second segment in which the coefficient of friction varied slowly with displacement (Figure 16). These two segments were joined by a segment in which the rate of increase of μ declined steadily with displacement. The variations in imposed slip rate caused changes in the friction coefficient that are superimposed on these longer term effects. In some experiments, stable sliding was interrupted by stick-slip events.

The varying normal stress during the transient decay of μ after a step in slip rate (Figure 16) may result in lengthening the transient. In order to test this, an experiment was performed in which the confining pressure was servo-controlled to maintain constant

normal stress. Both μ and the normal stress, σ_n, are plotted in Figure 17 for this experiment on dry Westerly granite gouge at 500 MPa normal stress. The transient effect shown does not differ in magnitude or length from the transients in runs for which the confining pressure was maintained constant (*Solberg*, unpublished data). Thus, based on this experiment at least, the varying normal stress does not cause a lengthening of the transient or affect the sign of the change in friction with change in sliding rate. (See Appendix I for further discussion.)

The coefficient of friction, μ, from two experiments is plotted against axial displacement in Figure 18. The confining pressure was 30 MPa in VF3 and 300 MPa in VF1. μ decreased with increasing normal stress on the sawcut. The linear portions of each plot of μ versus displacement were selected for determination of the changes in μ due to the variations in imposed slip rate. Each step in slip rate inaugurates a transient response of μ which, initially, always has the same sign as the slip rate change. $\Delta\mu$ for each step in slip rate was determined by extrapolating the friction plot from the previous increment of slip and subtracting that value from the current value of μ. Thus, the long-term variations in friction due to overall strain hardening or strain weakening are subtracted out.

Dieterich (1981) studied the distance (d_r) that the sample needed to slide after a change in velocity before short-term changes in friction have died off. He found that d_r varied with surface roughness and gouge grain size and was on the order of 0.1 to 0.2 mm for conditions similar to ours. We observed that sliding distances on the fault of 0.1 to 0.3 mm are required to allow these transients to decay and that d_r generally increased with increasing normal stress.

In addition to the effects of variations in slip rate, there were also changes in μ during sudden sliding events and their associated stress drops. Repeated stress drops occurred in run VF4 (Figure 19) at 300 MPa. These stress drops were initially separated by segments in which stable sliding occurred. However, as displacement increased, the frequency of stress drops became greater and stable sliding ceased. In contrast, run VF1, at 300 MPa, exhibited only one stress drop at a displacement of 9.8 mm. Figure 19 also indicates that the occurrence of stick-slip events is not necessarily related to changes in the imposed slip rate. For an axial displacement of 4 mm, a stick-slip event occurred near the end of the 7.33 μm/sec velocity step whereas the second stick-slip event occurred during the increase in friction that followed the 3-decade increase in imposed slip rate (Figure 19). All three stick-slip events shown in Figure 19 occurred during the highest imposed slip rate but a stick-slip event in run VF3 (Figure 18) occurred at the lowest imposed slip rate.

Determinations of B are plotted as a function of normal stress in Figure 20. Slip rate sensitivity of μ is positive and is in good agreement with B values measured under room-dry conditions by *Solberg and Byerlee* (1984). The slip rate sensitivity is not dependent on the sign of the slip rate change. For example, discounting the instability in VF4, the two plots of μ versus displacement representing the forward and reverse slip rate sequences at 300 MPa show almost exactly reverse behavior (Figures 18 and 19).

Further Comments

Three features of these experiments are of interest when considering fault instability: (1) positive rather than negative values of B are observed; (2) there is a lack of correlation

of imposed slip rate changes with stick-slip events; and (3) there is a simultaneous increase of both the frequency of stick-slip events and the value of B with displacement (Figures 3 and 19).

It is possible to explain these observations by assuming that the observed instabilities are driven by stress inhomogeneities related to cocking of the sample column. This is a well-known problem of the triaxial test geometry and more work is needed to understand how it affects test results. At the same time, we would like to suggest an alternate explanation in which we assume that the observed instabilities are related to structures in the gouge zone. Stick-slip events are uncorrelated with induced changes in slip rate (point 2, above). Thus, while the structure in the sliding zone is sometimes stable with respect to large changes in sliding rate it may, at other times, be so unstable that no externally-imposed slip rate changes are necessary to initiate instability. In contrast, sudden events are triggered at the time of the imposed velocity changes in the velocity-controlled model (*Tullis et al.*, 1985 and personal communcation). Regarding point 3 above, the increasing frequency of stick-slip events with displacement (Figure 19) suggests an evolution of the structure of the sliding zone. Structures that promoted stable sliding in the early portion of the VF4 experiment were steadily replaced by structures that could only fail catastrophically. At the same time, the slip rate sensitivity became more positive and Figure 3 indicates a general tendency towards greater positive values of B with displacement. Considering the velocity-dependent model of instability (*e.g., Rice and Ruina*, 1983), the structural changes that occurred in the sliding zone, causing the increase of B, should have prompted greater stability, a prediction that does not fit the observed behavior. Instead, the observed behavior was increasingly unstable. Velocity- and history-dependent friction laws might be extended to include purely displacement-dependent terms as well, although the complications involved may prove intractable for complex faults. One problem concerns the combination of spatial variation and continuing evolution of the friction coefficient.

A detailed study of the structural changes that occur in gouge during stable sliding and stick-slip (*Engelder et al.*, 1975; *Byerlee et al.*, 1978) reveal that the physical processes occurring during sliding are complex. Shear zones are developed oblique and parallel to the plane of the sawcuts. The results indicate that shearing oblique to the fault precedes sudden slip which is confined to the margins between the intact rock and gouge. Our present results suggest that when this transition occurs the friction force suddenly drops to produce the instability. It also seems that the degree of compaction of the gouge is an important factor because the instabilities have larger stress drops at higher normal stress and the distance of stable sliding before the instabilities decrease at greater displacement. Under these conditions the gouge is most dense.

In our experiments, the surfaces between the rock and gouge were flat and finely ground. Some sections of natural faults may also have curvature of the surfaces smaller than the width of the gouge. In this case, if sliding during an earthquake is confined to one of these sections, then we may expect instabilities on the fault to occur in much the same way as they did in our experiments. In many situations, however, the fault is not straight. The structure is exceedingly complex, and detailed studies of the geometry have shown that the surfaces are fractal over the entire band from 10^5 m to 10^{-5} m (*Scholz and Aviles*, 1986). *Byerlee* (1967) modeled a complex structure such as this by sliding on an

irregular but completely interlocked surface at high pressure and found that the friction decreased with displacement as the irregularities on the surface fractured. This led to stick-slip as the displacement-dependent model, suggested by *Byerlee* (1970), predicts. In those experiments the surfaces developed a layer of fault gouge as the irregularities became ground up. Such a process must be occurring on natural faults as well because the width of the breccia and gouge zone increase with displacement between the surfaces (*Wallace and Morris*, 1979; *Robertson*, 1983).

This cannot be the only process involved, because if it were, the fault would get smoother. Faults such as the San Andreas that have slid for great distances over millions of years are exceedingly complex (*Sibson*, 1986; *King*, 1986; *King and Nabeleck*, 1985; *Segall and Pollard*, 1980). Thus there must also be a roughening process occurring which will increase the frictional strength as the surfaces slide past one another. How this may occur can be explained in the following way. In studying the surfaces of glass developed during tension fracture, it is observed that at low crack velocity the surfaces are smooth while at high velocity they have irregularities that are caused by the interference of the crack front with the elastic waves radiated by the fracture itself (*McClintock and Argon*, 1966). In other words, the dynamic stress modifies the static stress field, resulting in a total stress which is in a direction different from the static stress direction. As a result, the crack is momentarily deflected from its overall propagation direction. Such a process may also occur during the growth of the shear fracture plane during slip on natural faults provided that the strength of the rock in the new direction does not exceed the driving stress.

It has often been assumed that the complexity of the seismic wave is due to the rupture of preexisting interlocked asperities as the fracture grows (*Kanamori and Stewart*, 1978; *Choy and Boatwright*, 1981; *Boatwright*, 1984), but much of the complexity may also be due to the fracture of asperities that were not previously in contact and the development and fracture of newly generated asperities as the fault slips. This physical process is well characterized by a dynamic rupture model in which friction varies with displacement to produce the complex seismic wave of an earthquake and which maintains a complex geometry during repeated slip on the fault.

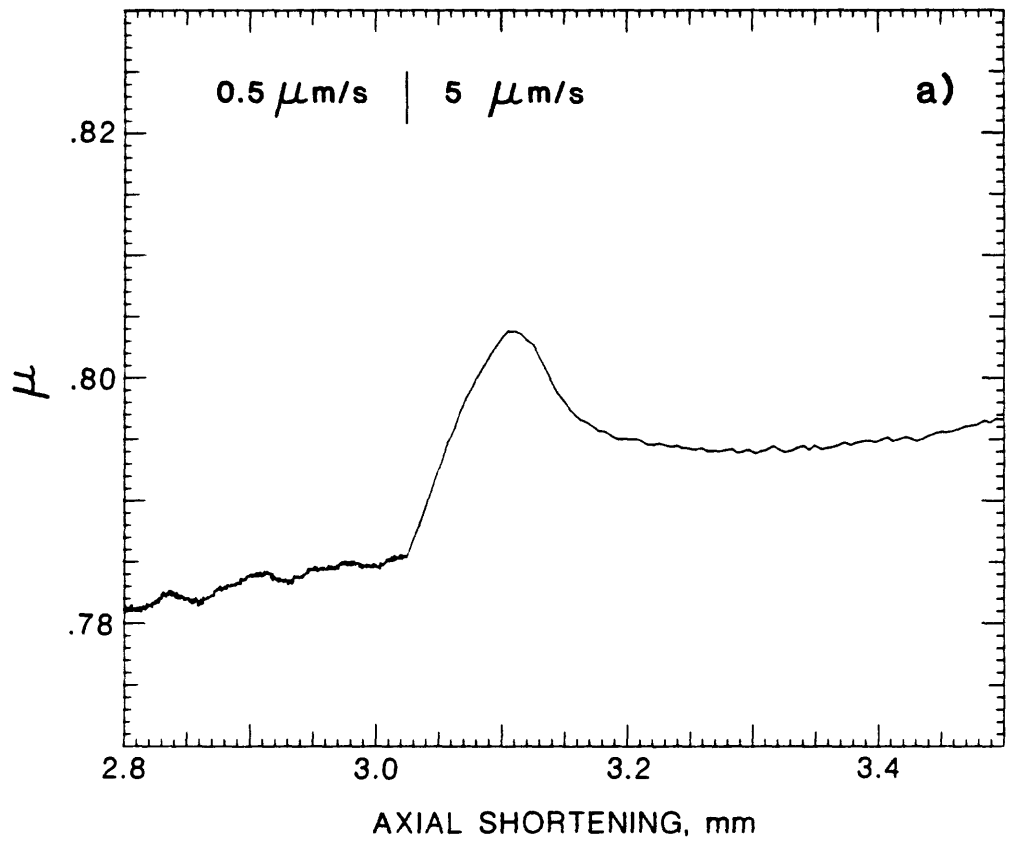
0.5 μm/s | 5 μm/s
a)
.82
.80
.78
μ
2.8
3.0
3.2
3.4
AXIAL SHORTENING, mm

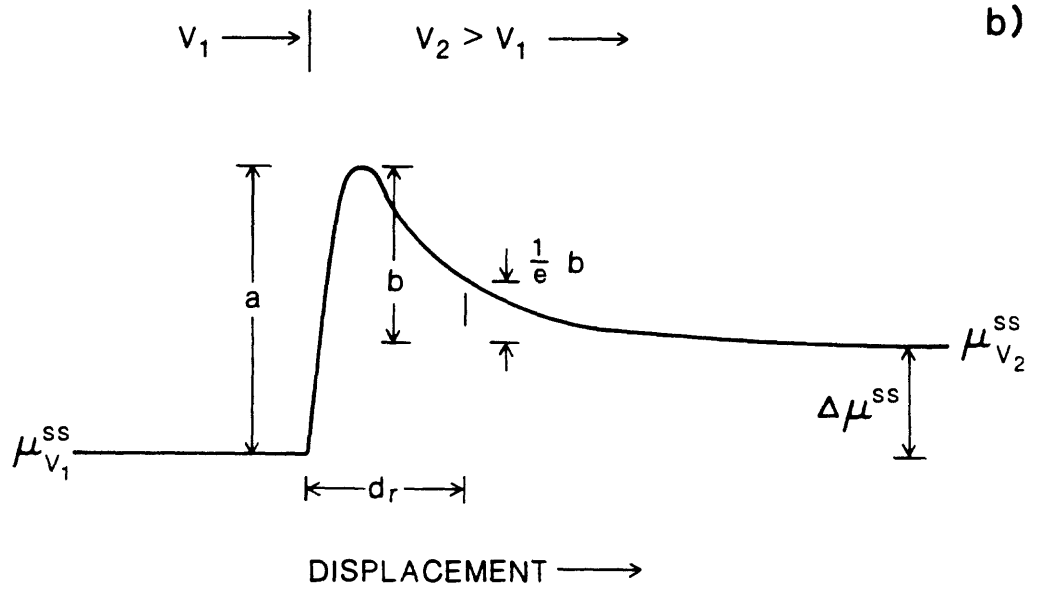
V1 →
V2 > V1 →
b)
a
b
1/e b
$\mu^{ss}_{V_1}$
$\mu^{ss}_{V_2}$
$\Delta\mu^{ss}$
dr
DISPLACEMENT →

FIGURE 1

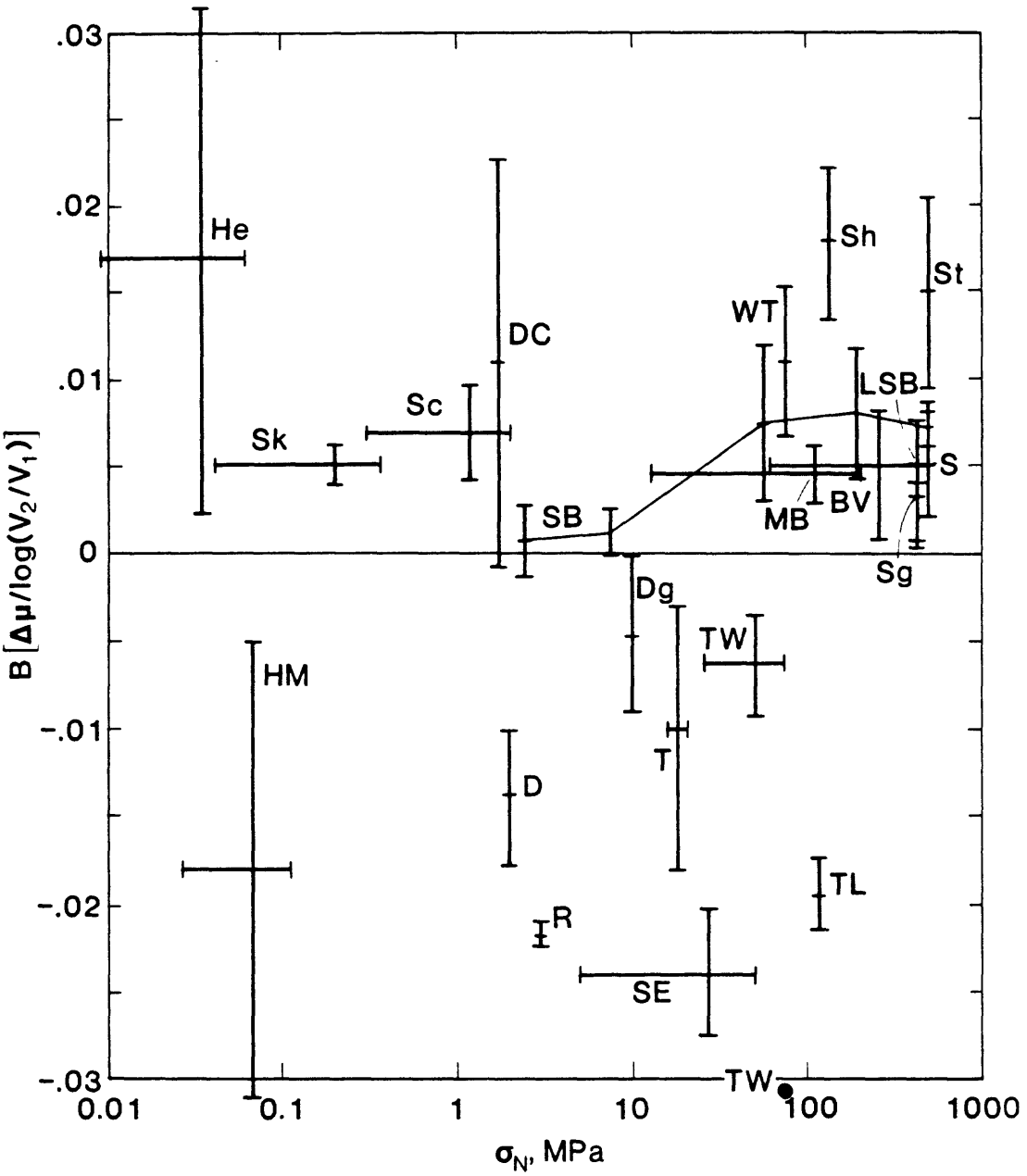
.03
.02
.01
0
-.01
-.02
-.03
B [Δμ/log(V2/V1)]
0.01
0.1
1
10
100
1000
σN, MPa
He
Sk
Sc
DC
SB
Sh
St
WT
LSB
S
BV
MB
Sg
Dg
TW
HM
T
D
TL
R
SE
TW

FIGURE 2

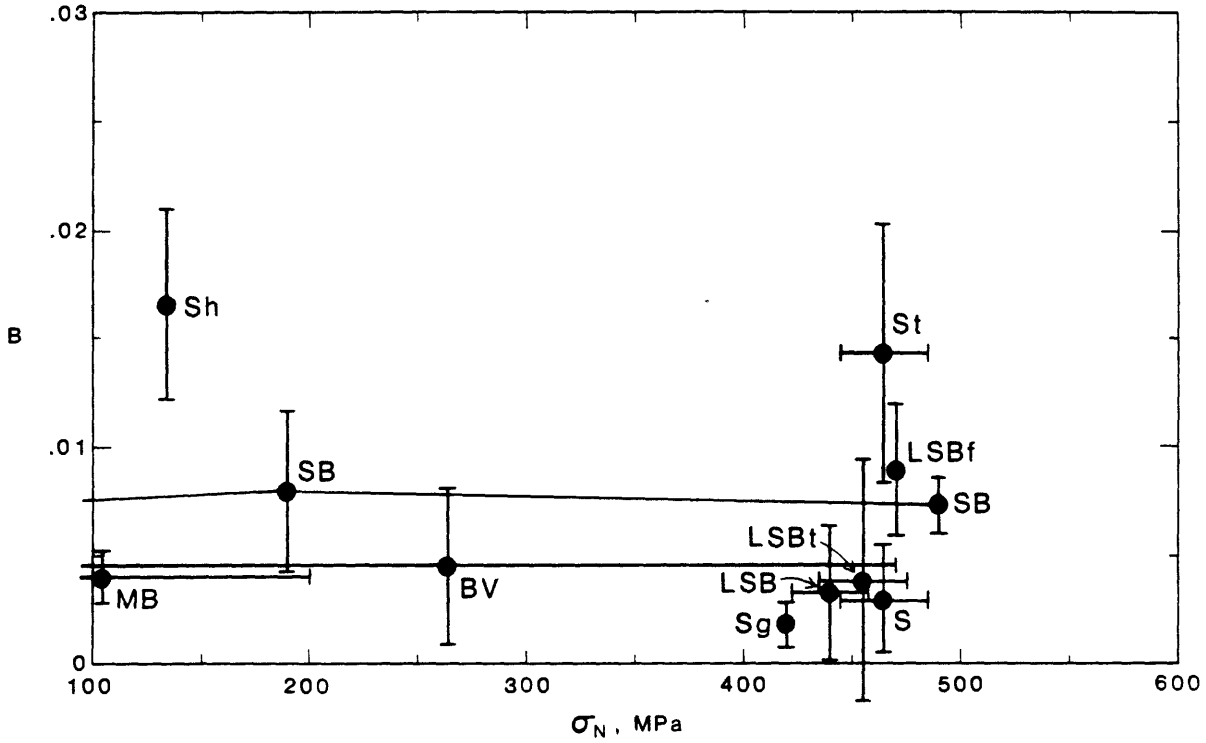
.03
.02
.01
0
B
Sh
SB
MB
BV
St
LSBf
SB
LSBt
LSB
Sg
S
100
200
300
400
500
600
σ_N, MPa

FIGURE 2A

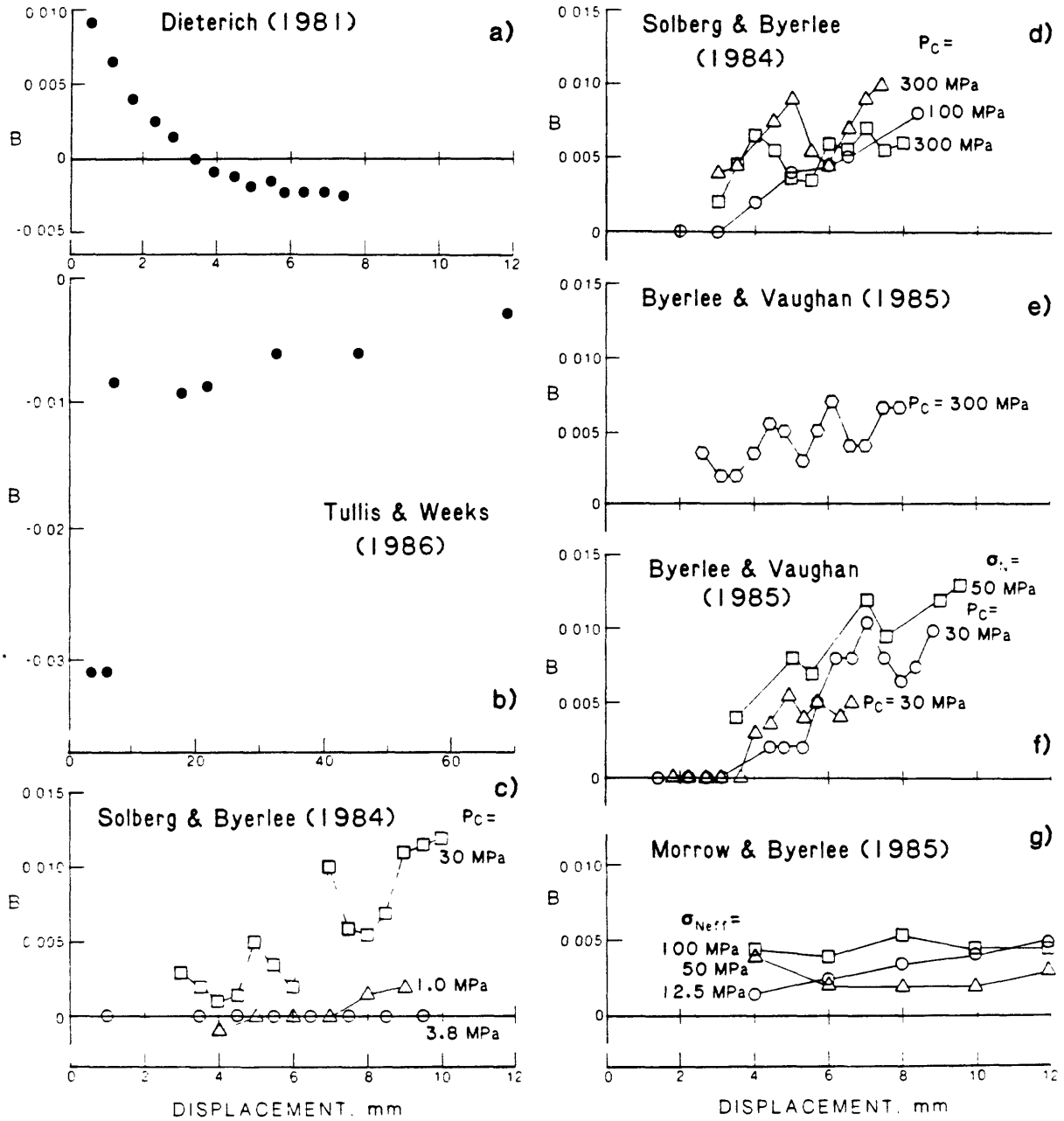
Dieterich (1981)
a)
B
Tullis & Weeks
(1986)
b)
Solberg & Byerlee (1984)
Pc=
30 MPa
1.0 MPa
3.8 MPa
c)
DISPLACEMENT, mm
Solberg & Byerlee
(1984)
Pc=
d)
300 MPa
100 MPa
300 MPa
Byerlee & Vaughan (1985)
e)
Pc = 300 MPa
Byerlee & Vaughan
(1985)
σn=
50 MPa
Pc=
30 MPa
Pc= 30 MPa
f)
Morrow & Byerlee (1985)
g)
σNeff=
100 MPa
50 MPa
12.5 MPa
DISPLACEMENT, mm

FIGURE 3

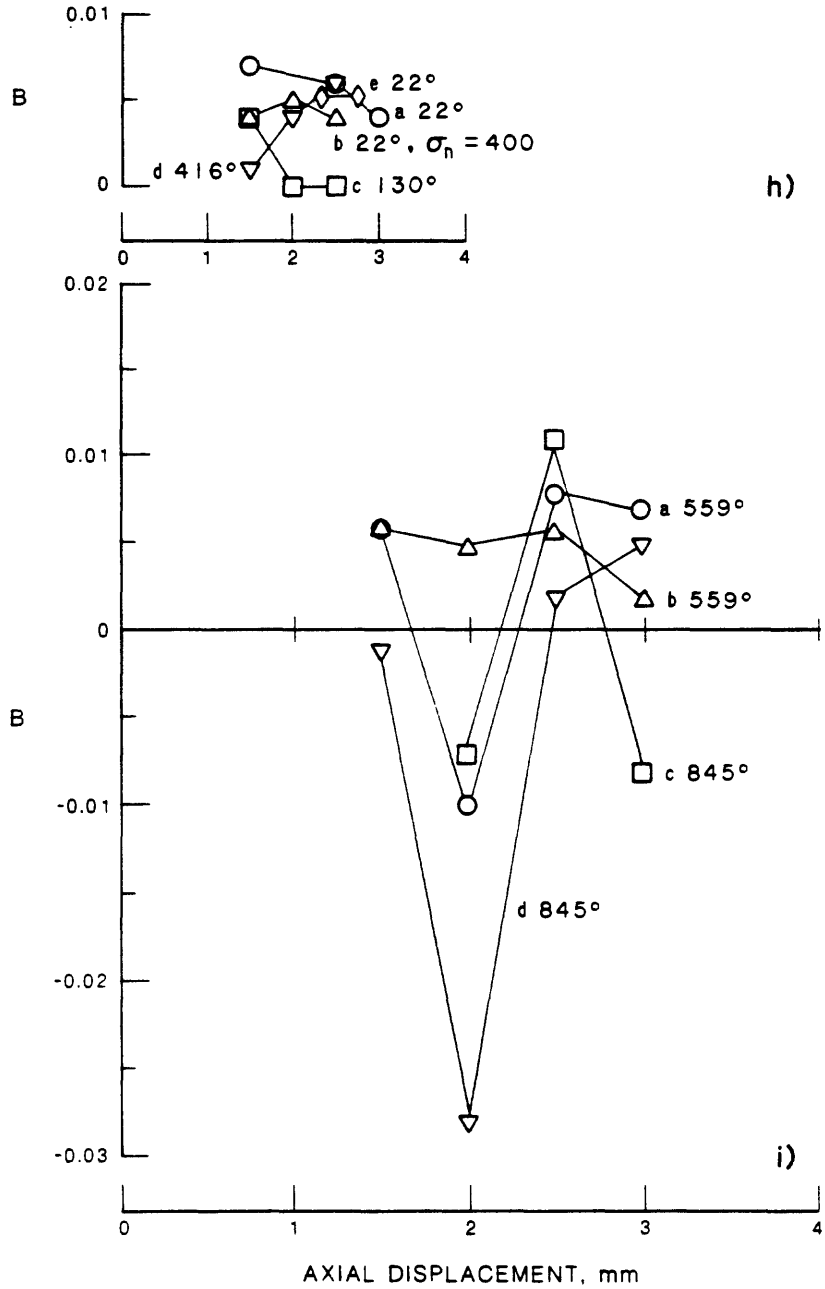

FIGURE 3 (CONTINUED)

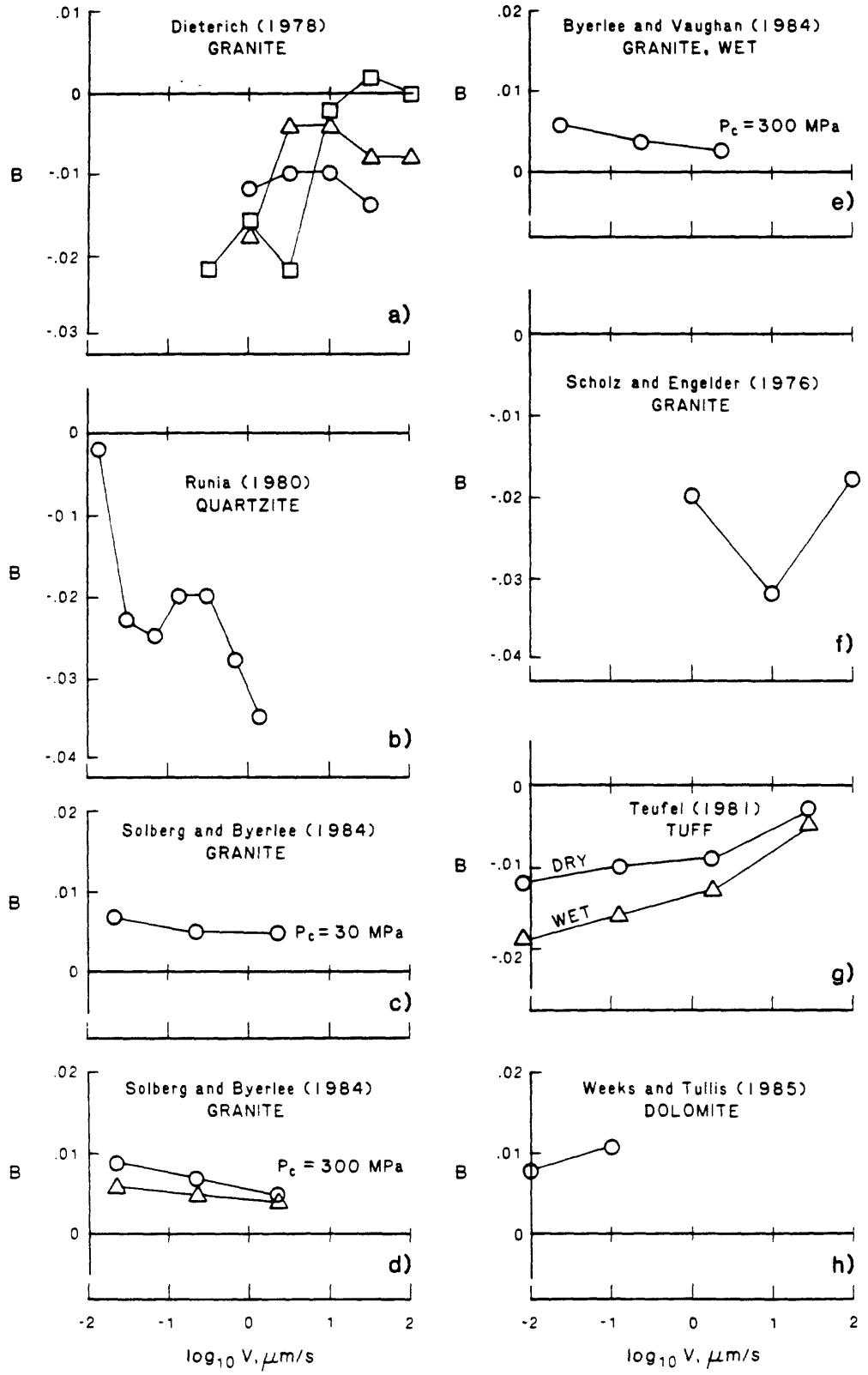
Dieterich (1978)
GRANITE
a)
Runia (1980)
QUARTZITE
b)
Solberg and Byerlee (1984)
GRANITE
P_c = 30 MPa
c)
Solberg and Byerlee (1984)
GRANITE
P_c = 300 MPa
d)
Byerlee and Vaughan (1984)
GRANITE, WET
P_c = 300 MPa
e)
Scholz and Engelder (1976)
GRANITE
f)
Teufel (1981)
TUFF
DRY
WET
g)
Weeks and Tullis (1985)
DOLOMITE
h)
B
$\log_{10}$ V, μm/s

FIGURE 4

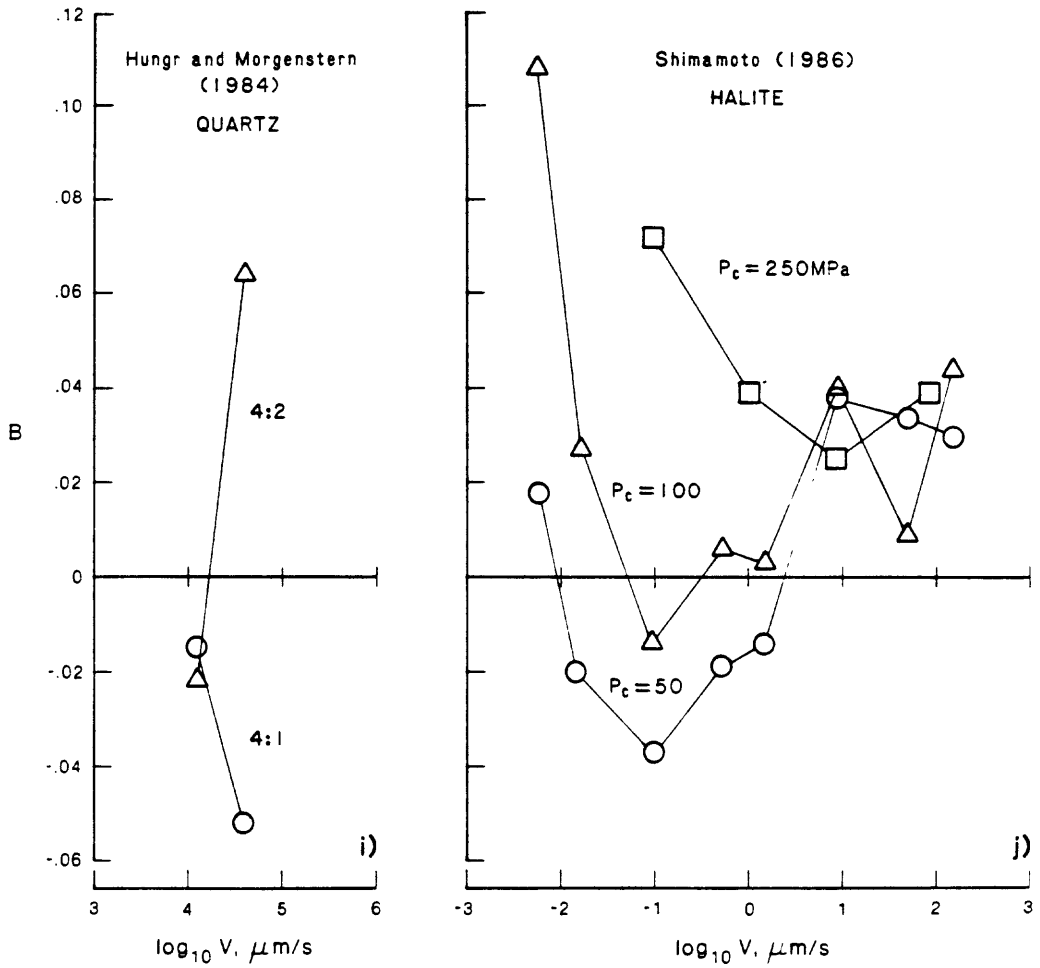

FIGURE 4 (CONTINUED)

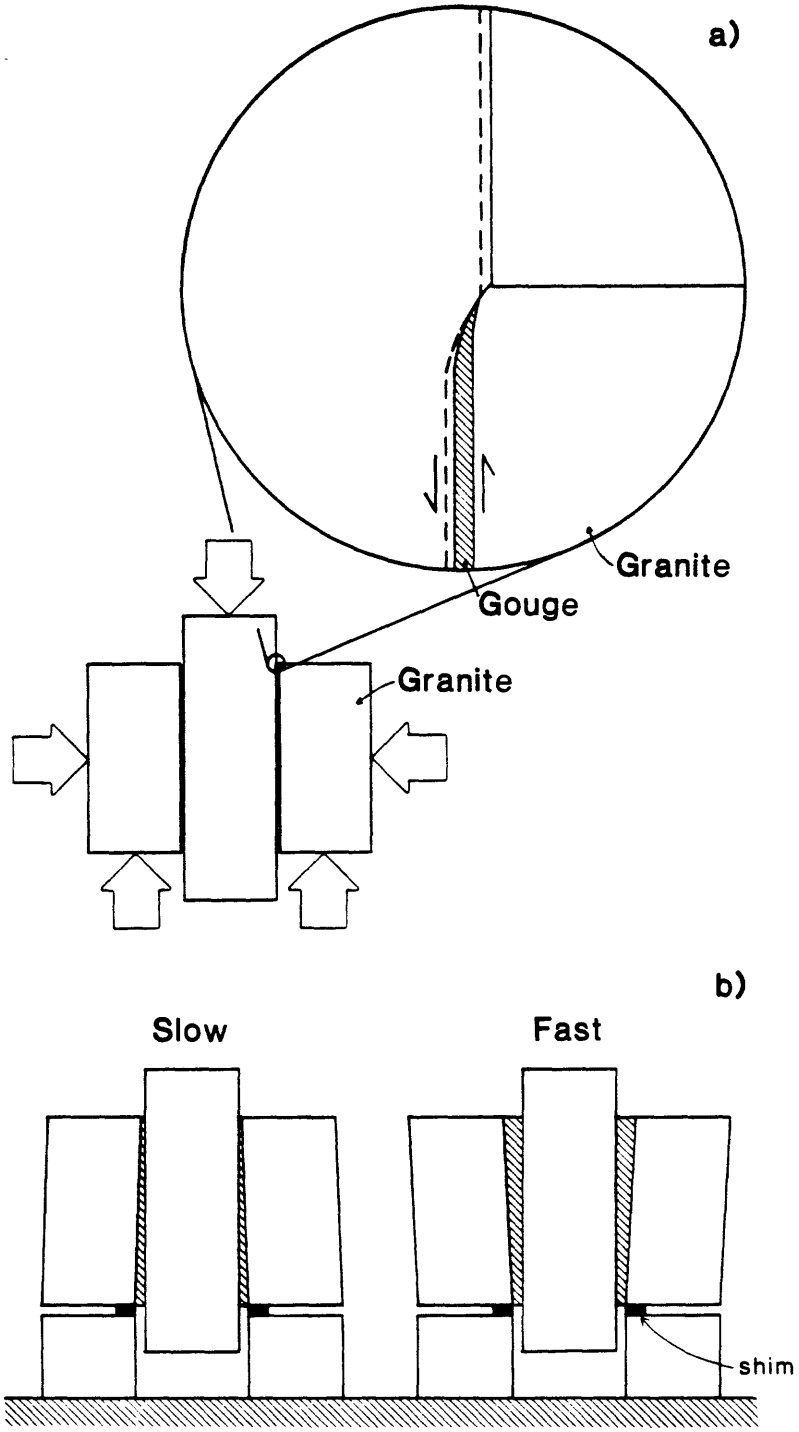

FIGURE 5

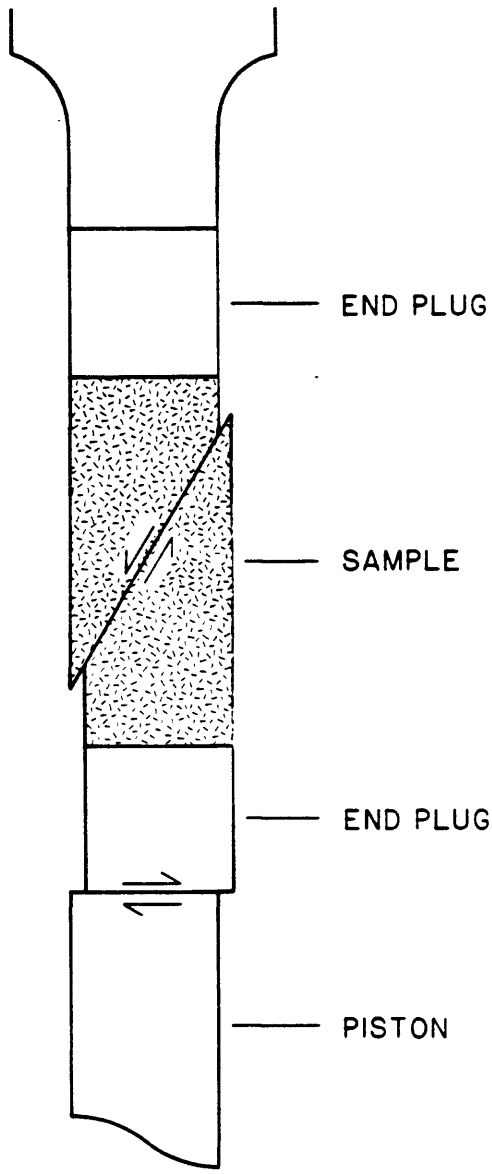

FIGURE 6

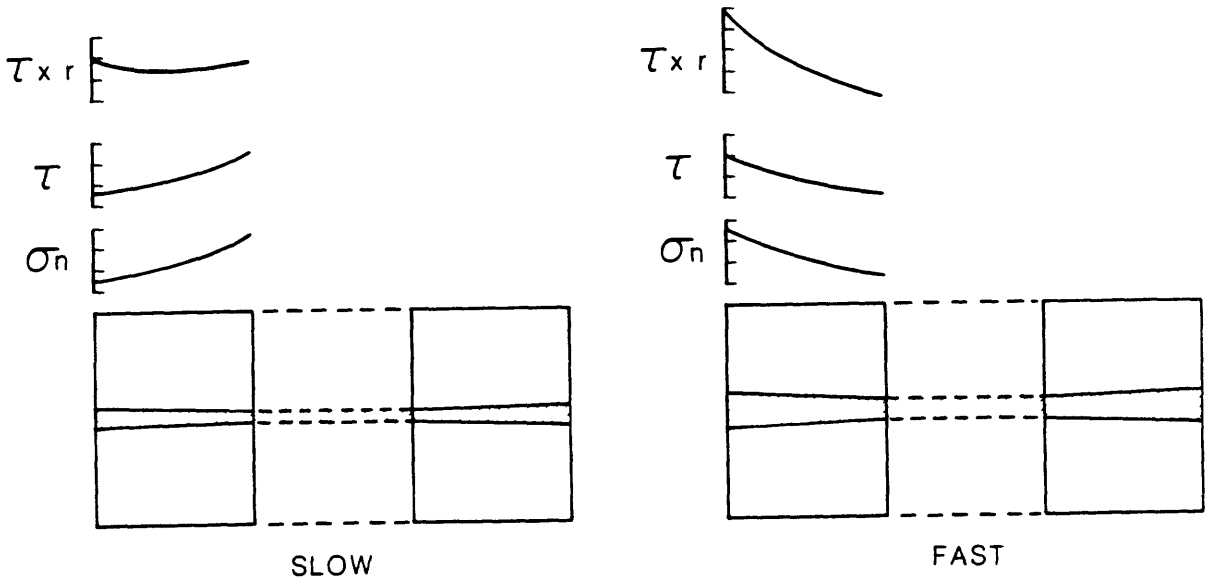

FIGURE 7

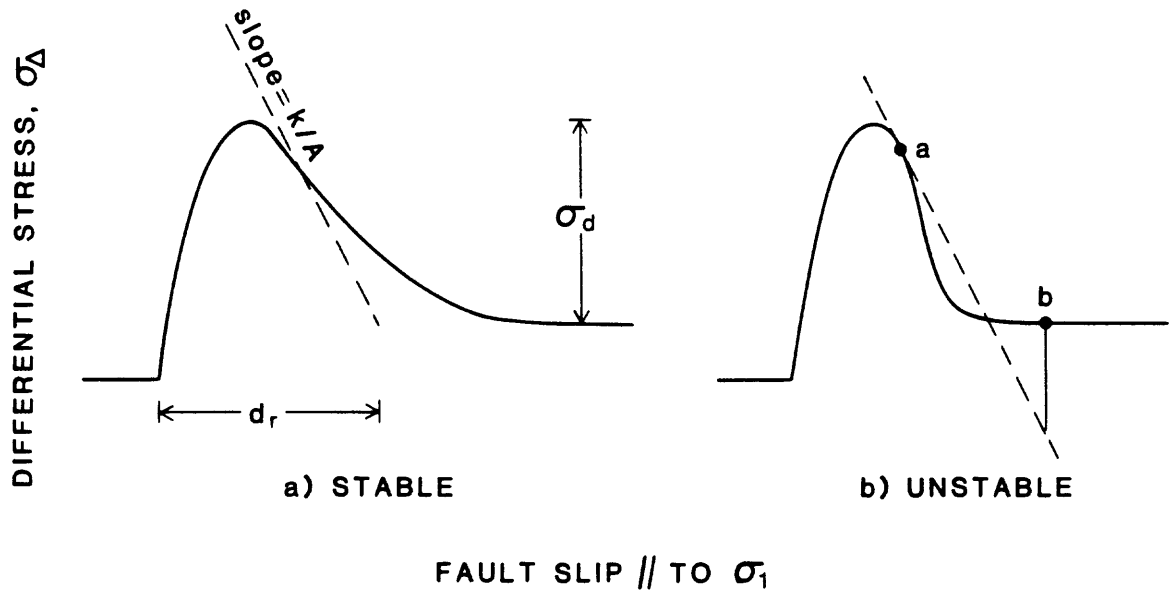
DIFFERENTIAL STRESS, σ_Δ
slope = k/A
σ_d
d_r
a
b
a) STABLE
b) UNSTABLE
FAULT SLIP // TO σ_1

FIGURE 8

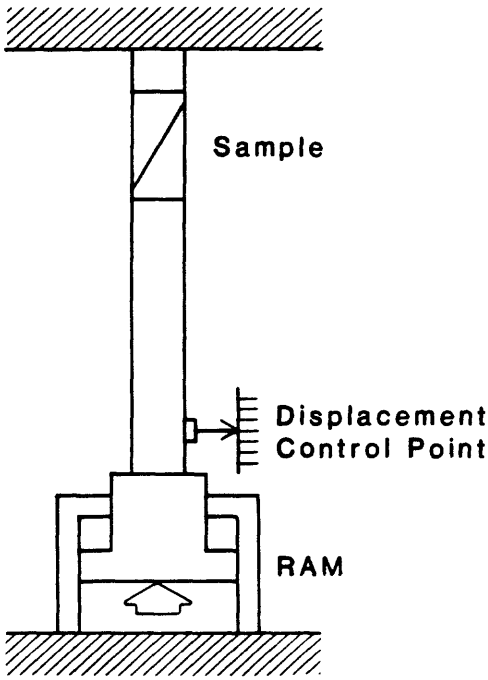

a)

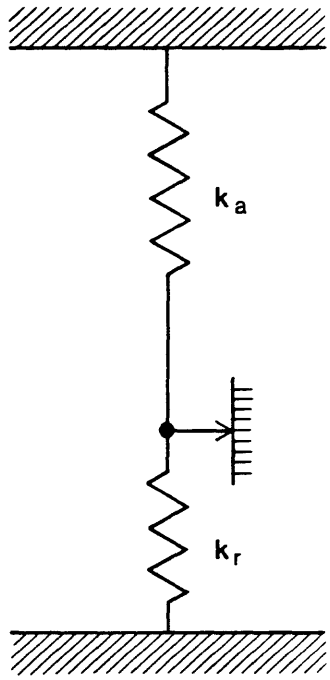

b)

FIGURE 9

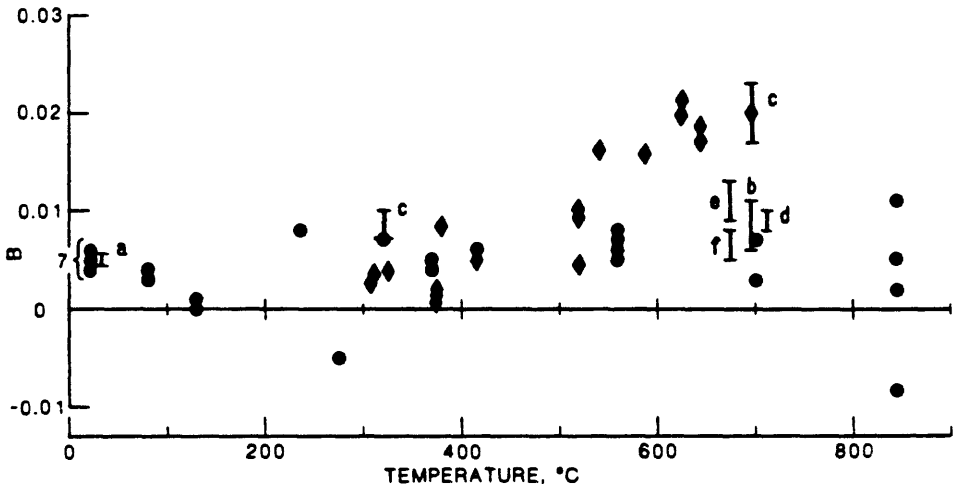

Figure 10

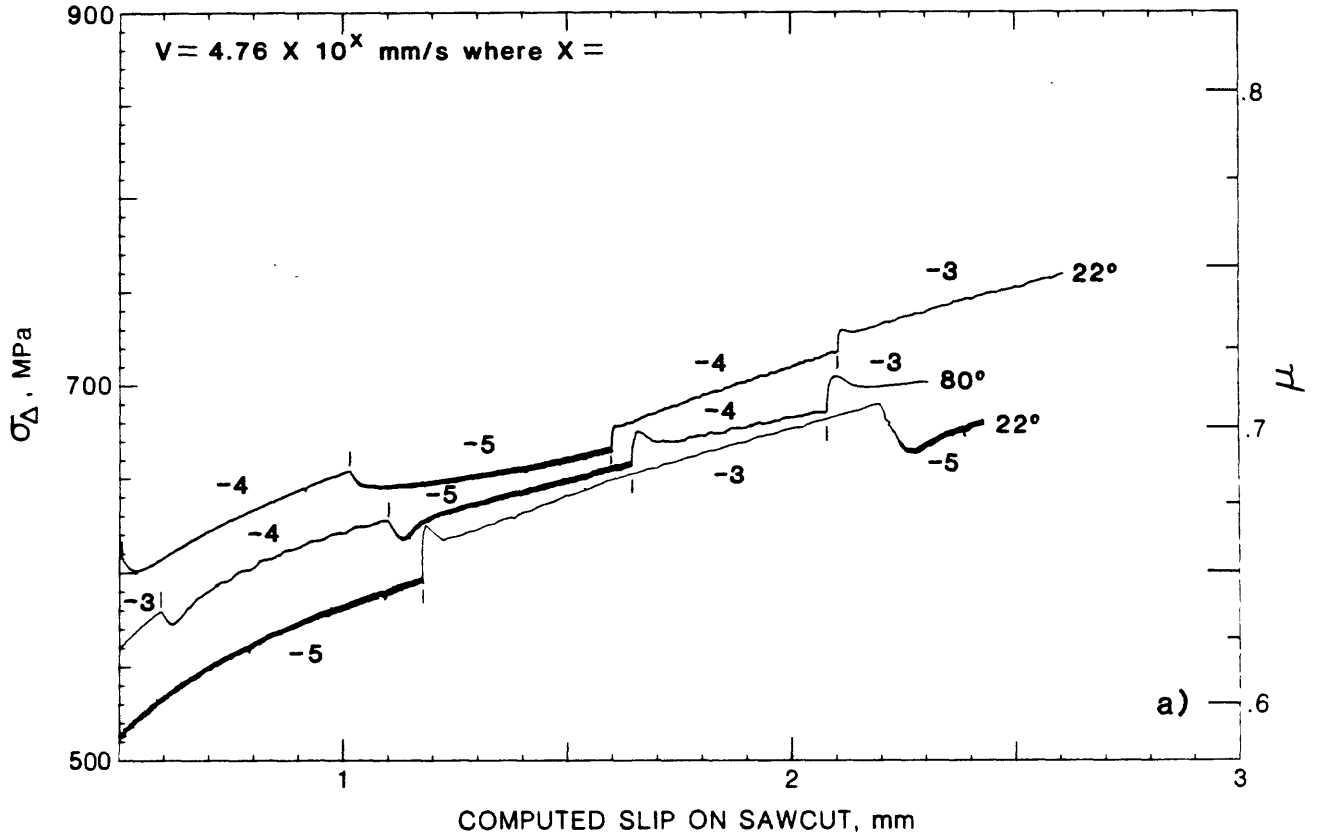
V = 4.76 X 10^X mm/s where X =
900
700
500
σΔ, MPa
.8
.7
.6
μ
1
2
3
COMPUTED SLIP ON SAWCUT, mm
-3
22°
-4
-3
80°
-4
22°
-5
-4
-5
-3
-4
-5
-3
-5
a)

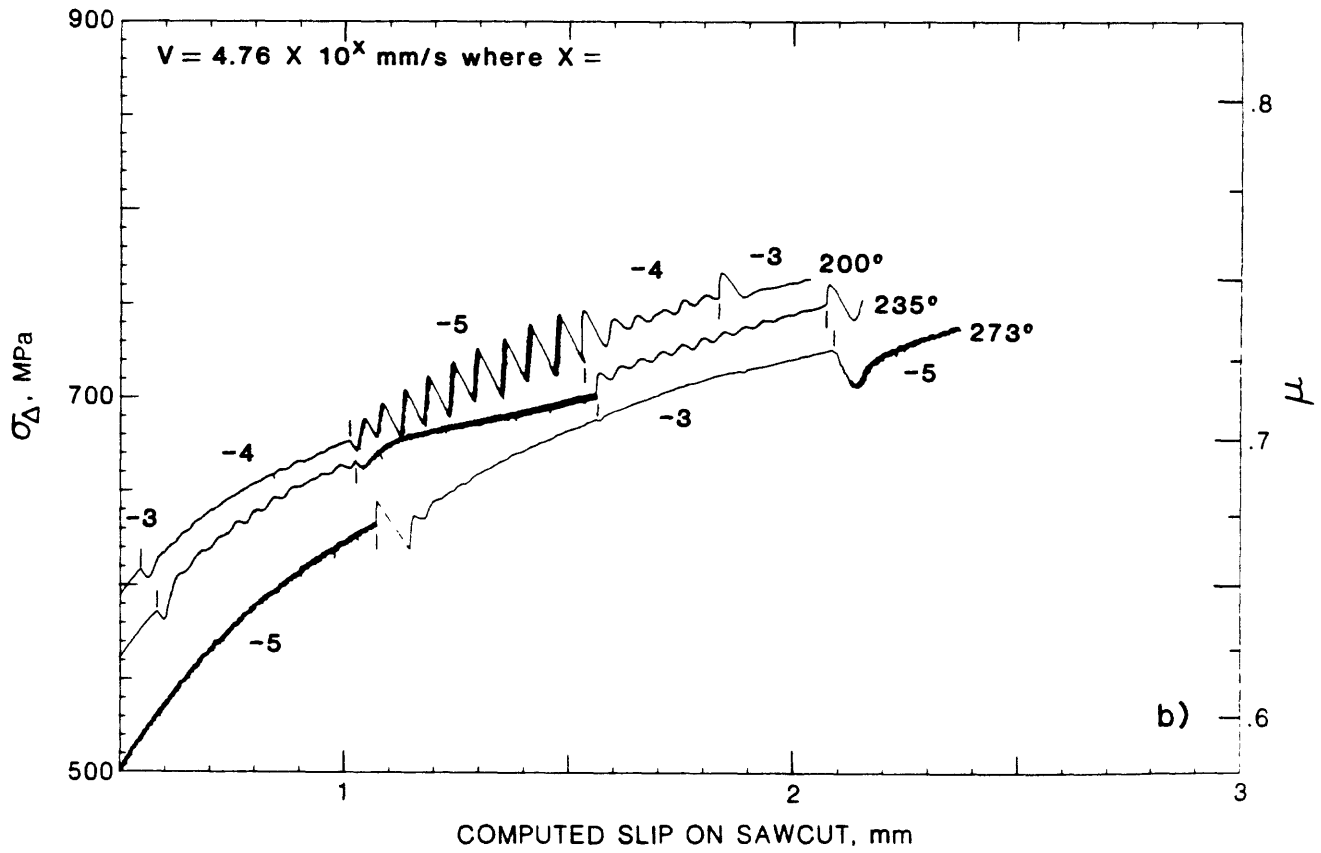
V = 4.76 X 10^X mm/s where X =
900
700
500
σΔ, MPa
.8
.7
.6
μ
1
2
3
COMPUTED SLIP ON SAWCUT, mm
-4
-3
200°
-5
235°
273°
-5
-3
-4
-3
-5
b)

FIGURE 11

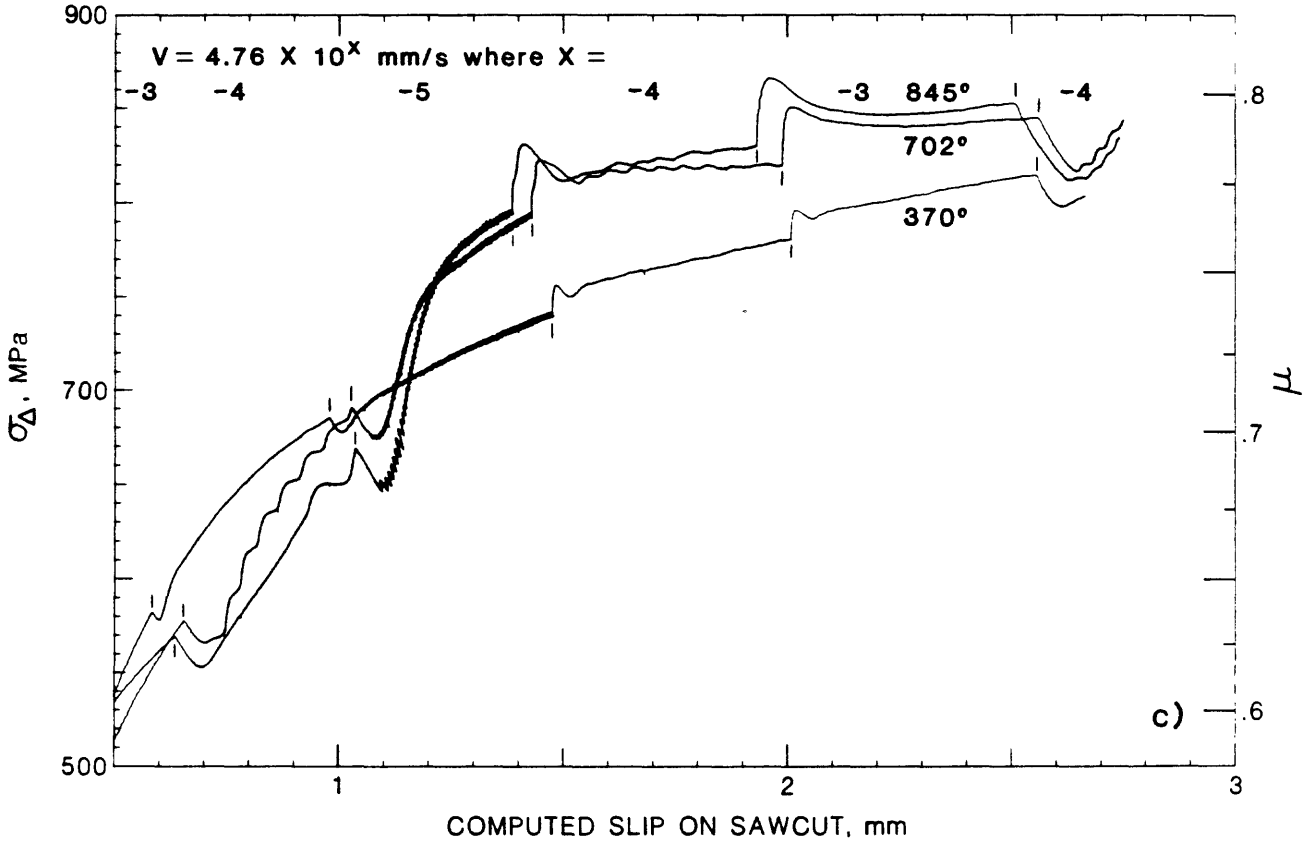

FIGURE 11 (CONTINUED)

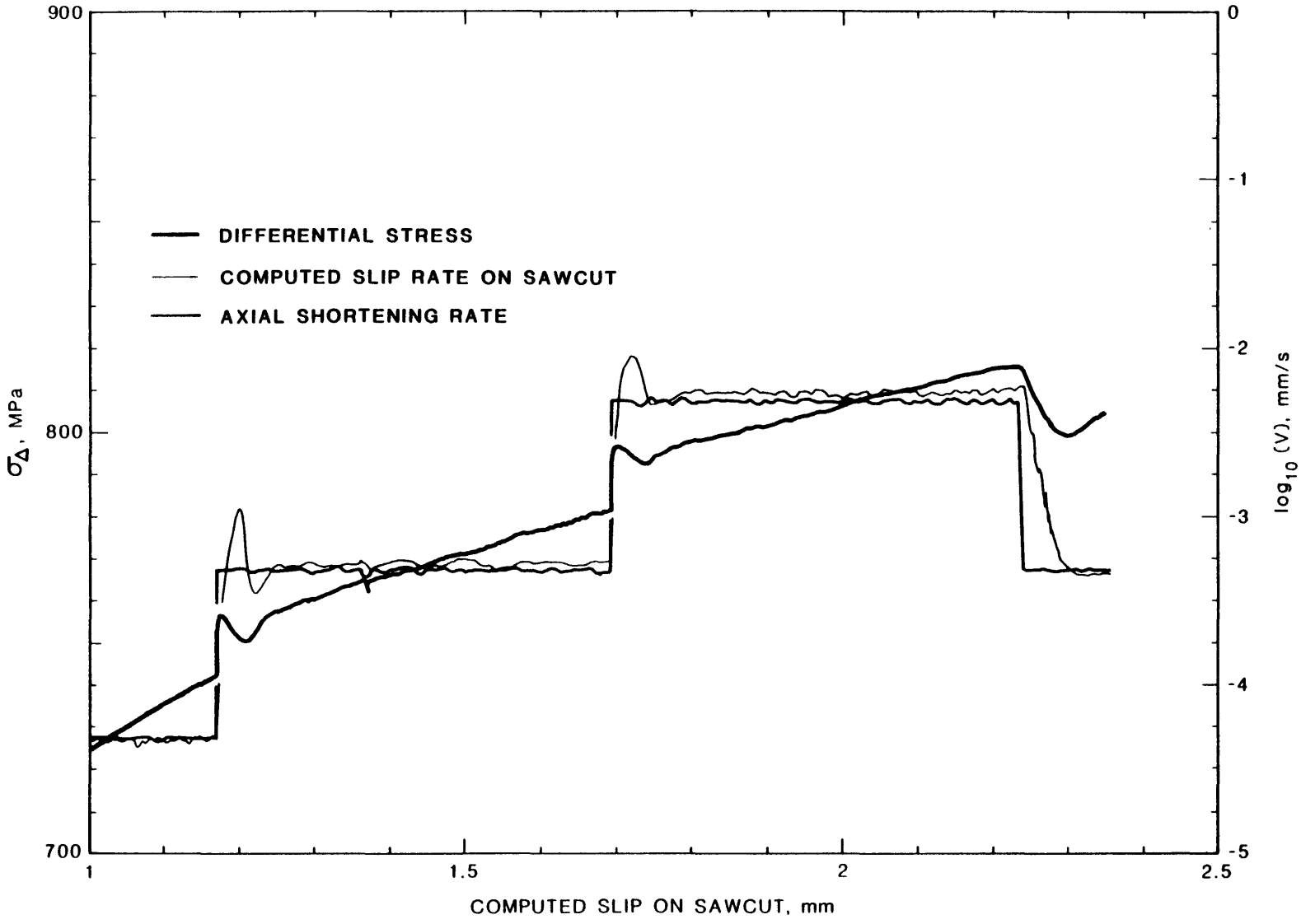
DIFFERENTIAL STRESS
COMPUTED SLIP RATE ON SAWCUT
AXIAL SHORTENING RATE
900
800
700
σ_Δ, MPa
0
-1
-2
-3
-4
-5
$\log_{10}$ (V), mm/s
1
1.5
2
2.5
COMPUTED SLIP ON SAWCUT, mm

FIGURE 12

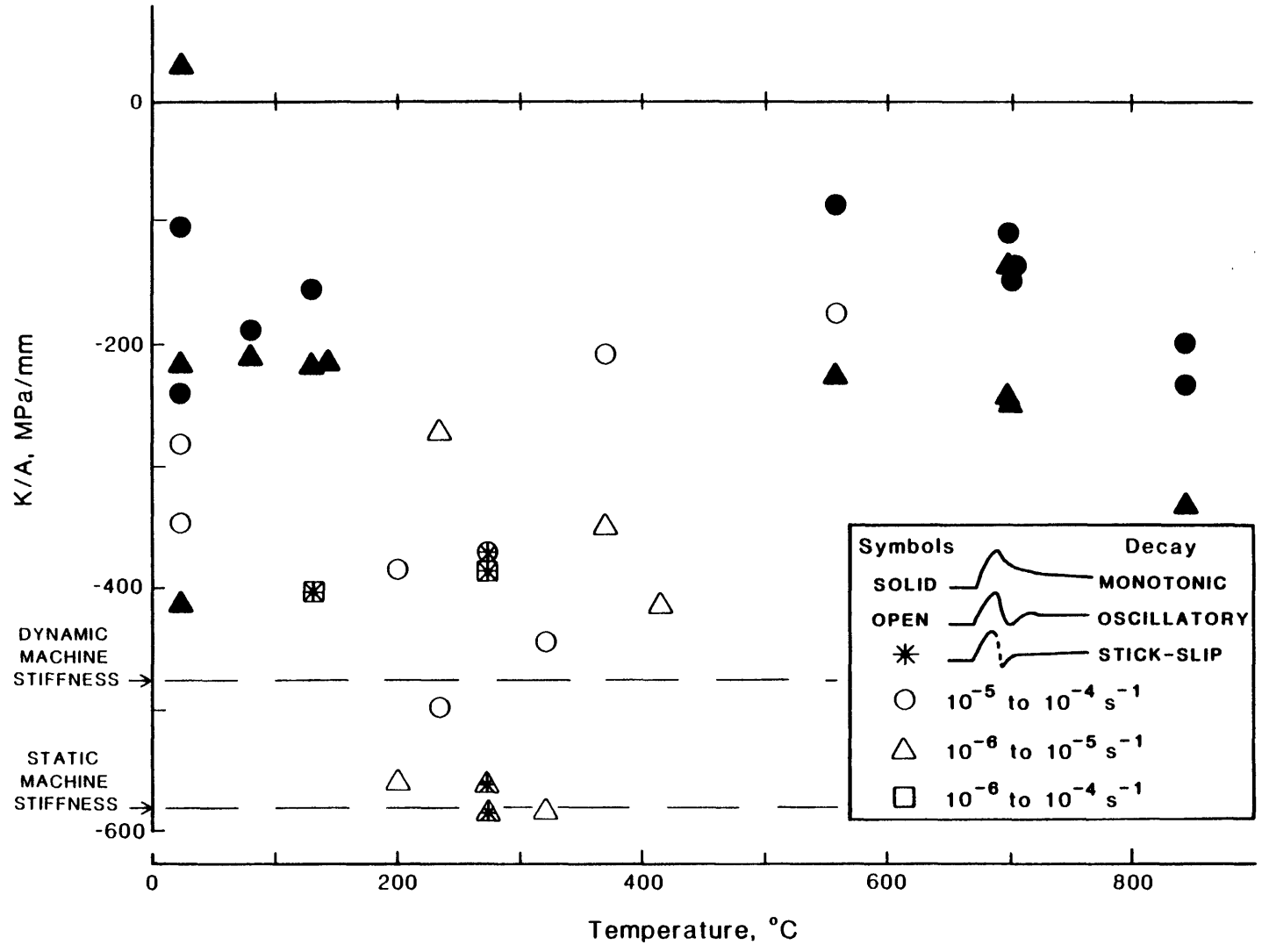
0
-200
-400
-600
K/A, MPa/mm
DYNAMIC MACHINE STIFFNESS
STATIC MACHINE STIFFNESS
0
200
400
600
800
Temperature, °C
Symbols
Decay
SOLID
MONOTONIC
OPEN
OSCILLATORY
STICK-SLIP
10^-5 to 10^-4 s^-1
10^-6 to 10^-5 s^-1
10^-6 to 10^-4 s^-1

FIGURE 13

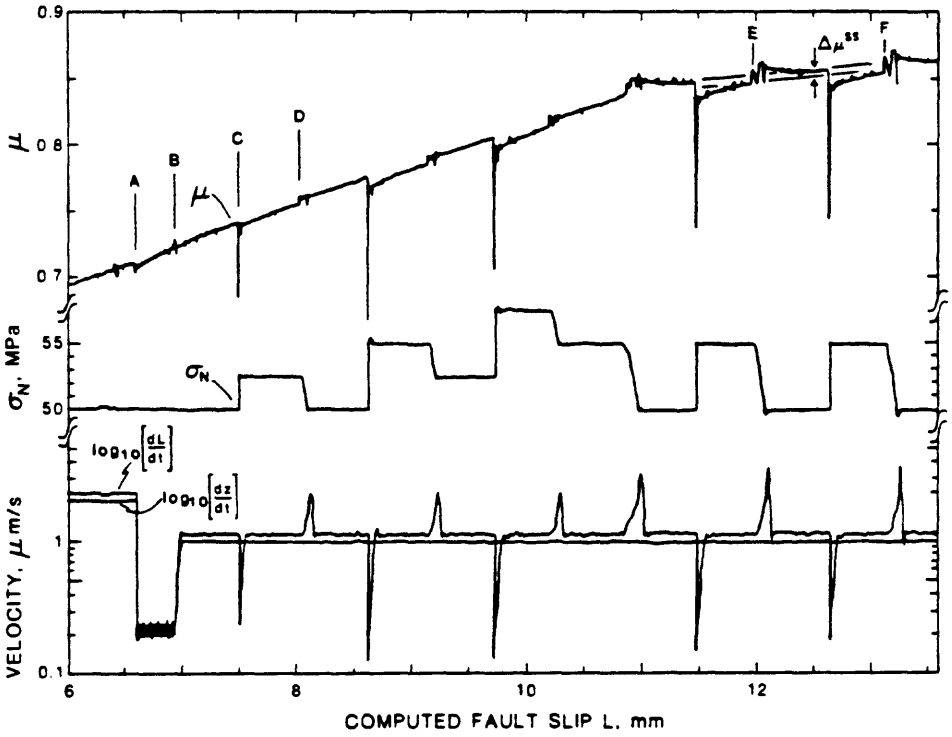
0.9
0.8
0.7
μ
A
B
C
D
E
F
Δμ^ss
μ
55
50
σN, MPa
σN
log10[dL/dt]
log10[dz/dt]
1
0.1
VELOCITY, μm/s
6
8
10
12
COMPUTED FAULT SLIP L, mm

Figure 14

SAMPLE ASSEMBLY

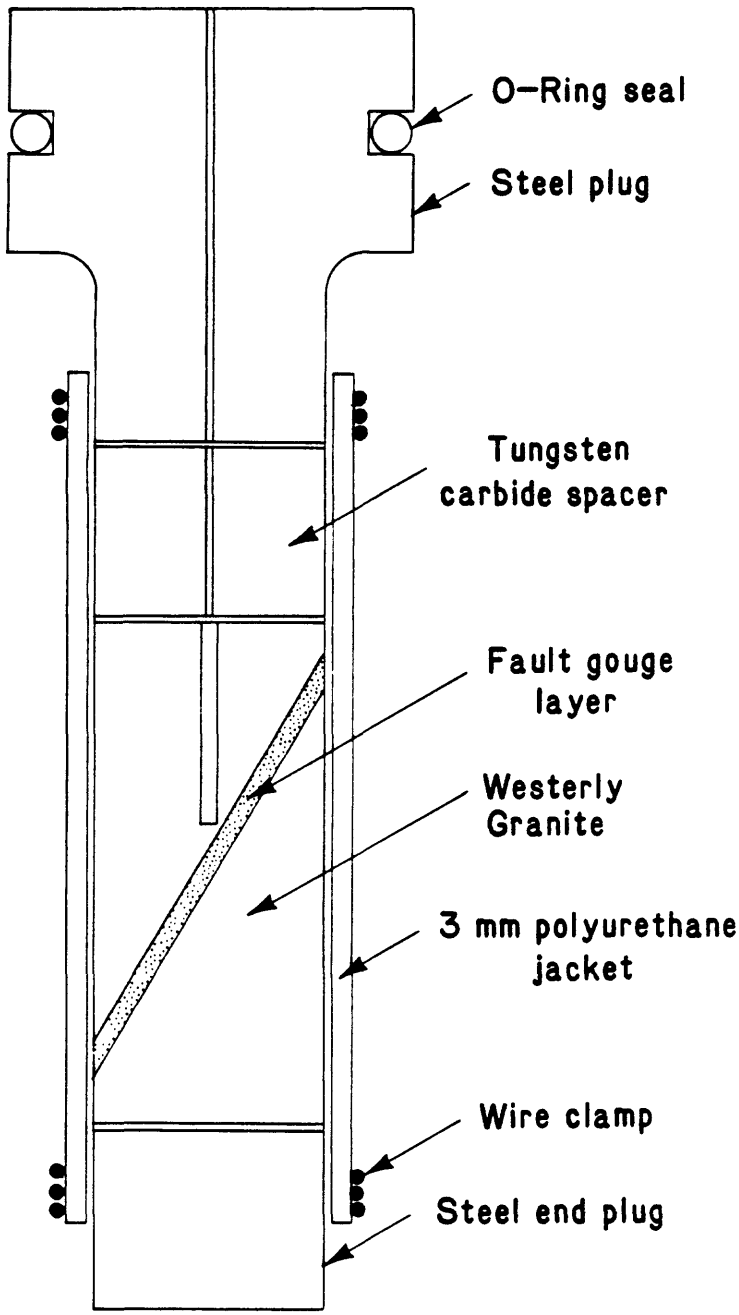

FIGURE 15

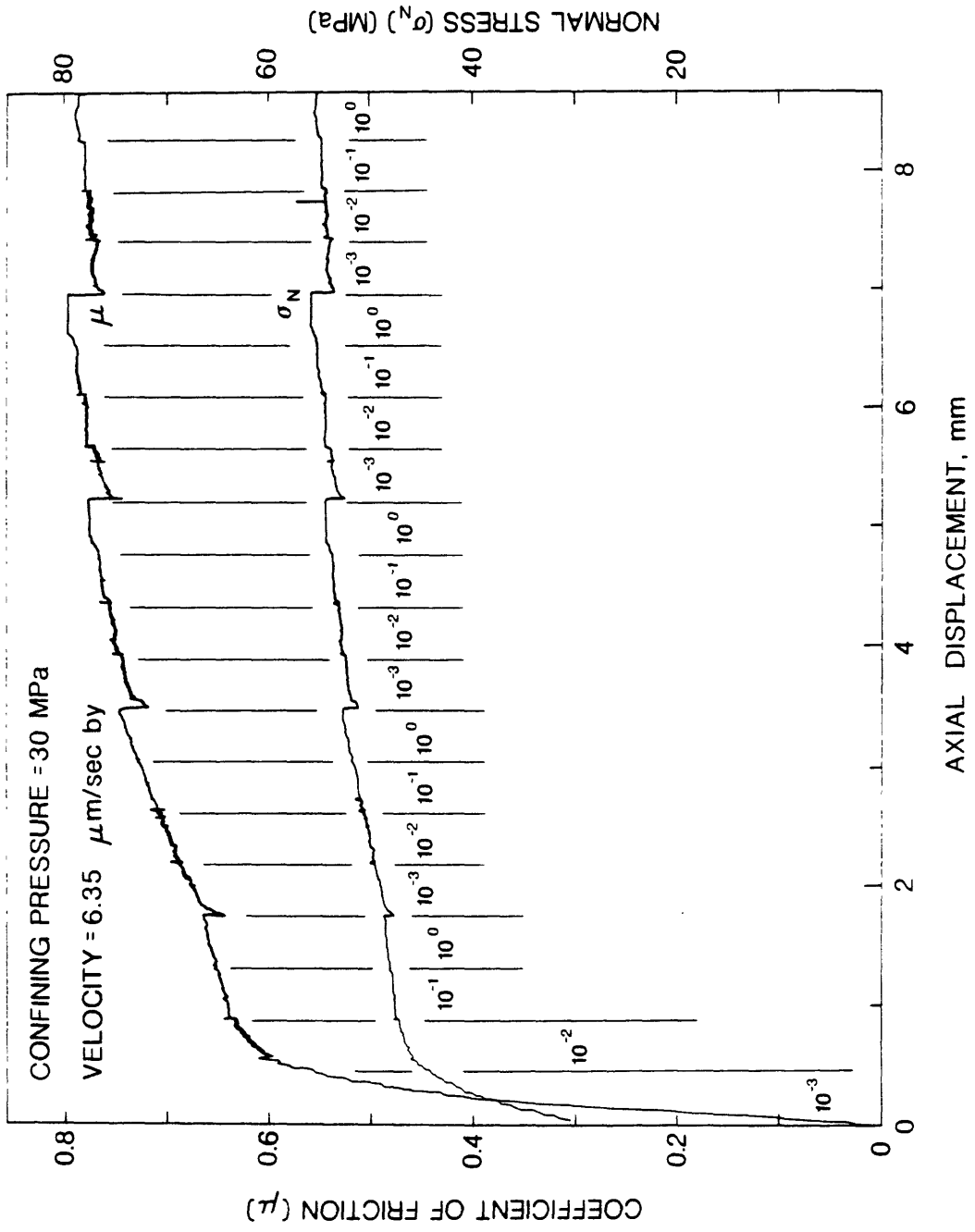
CONFINING PRESSURE = 30 MPa
VELOCITY = 6.35 μm/sec by
μ
σN
10-3
10-2
10-1
100
COEFFICIENT OF FRICTION (μ)
NORMAL STRESS (σN) (MPa)
AXIAL DISPLACEMENT, mm
0
0.2
0.4
0.6
0.8
20
40
60
80
2
4
6
8

FIGURE 16

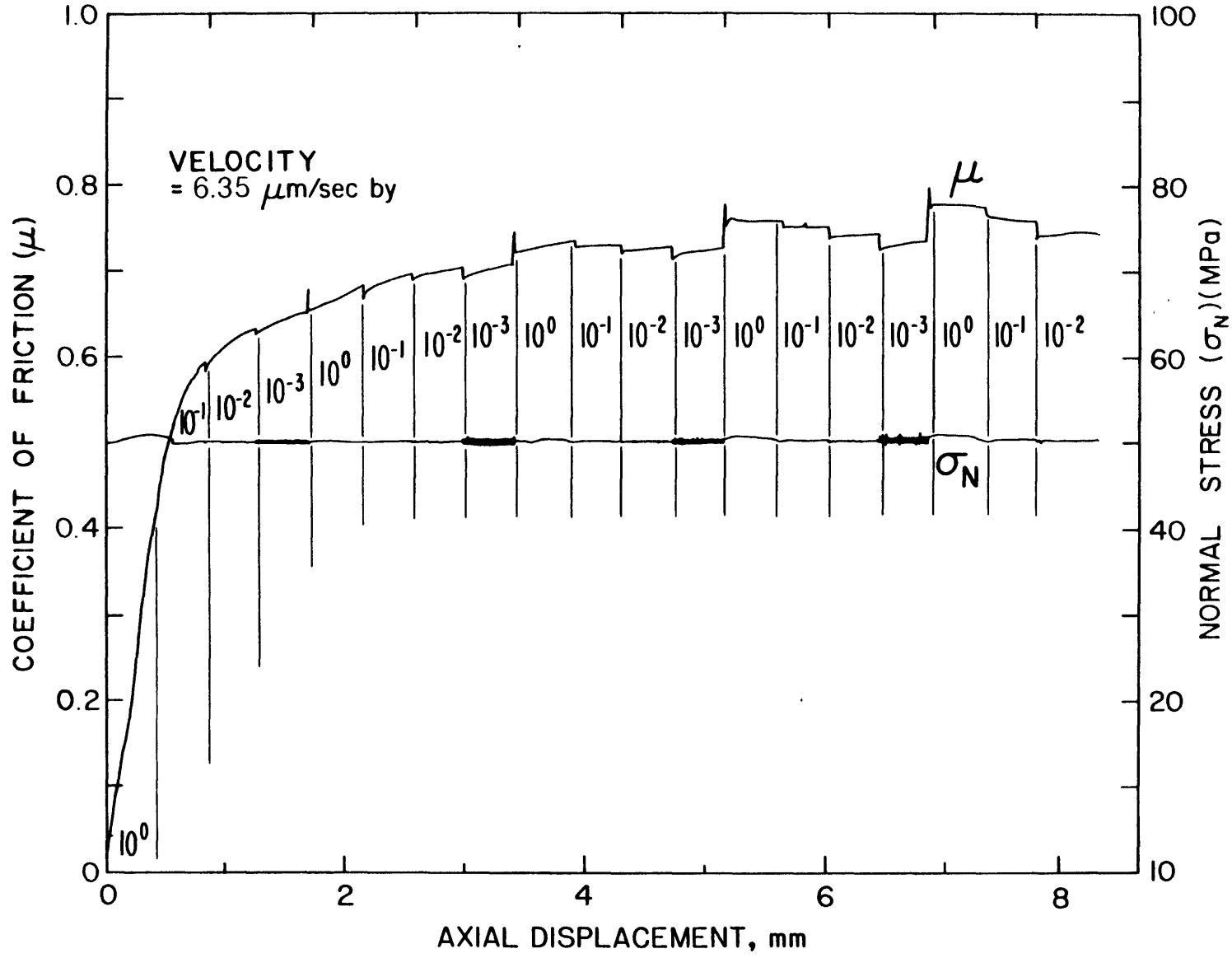
VELOCITY
= 6.35 μm/sec by
μ
σN
COEFFICIENT OF FRICTION (μ)
NORMAL STRESS (σN)(MPa)
AXIAL DISPLACEMENT, mm
1.0
0.8
0.6
0.4
0.2
0
100
80
60
40
20
10
0
2
4
6
8
10^0
10^-1 10^-2 10^-3 10^0 10^-1 10^-2 10^-3 10^0 10^-1 10^-2 10^-3 10^0 10^-1 10^-2 10^-3 10^0 10^-1 10^-2

FIGURE 17

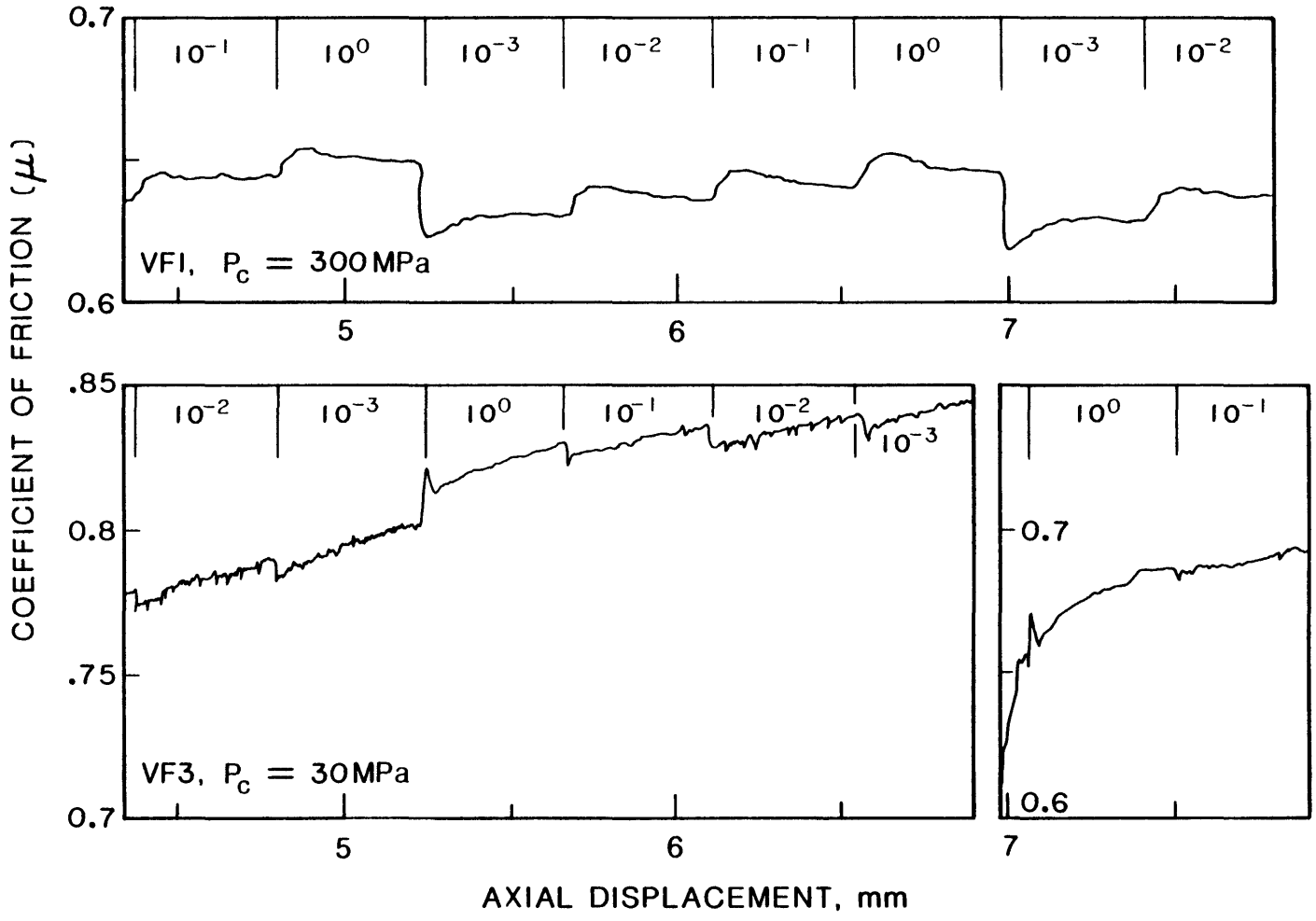
0.7
0.6
10^{-1} 10^{0} 10^{-3} 10^{-2} 10^{-1} 10^{0} 10^{-3} 10^{-2}
VF1, P_c = 300MPa
5
6
7
.85
0.8
.75
0.7
10^{-2} 10^{-3} 10^{0} 10^{-1} 10^{-2} 10^{-3}
VF3, P_c = 30MPa
10^{0} 10^{-1}
0.7
0.6
COEFFICIENT OF FRICTION (μ)
AXIAL DISPLACEMENT, mm

FIGURE 18

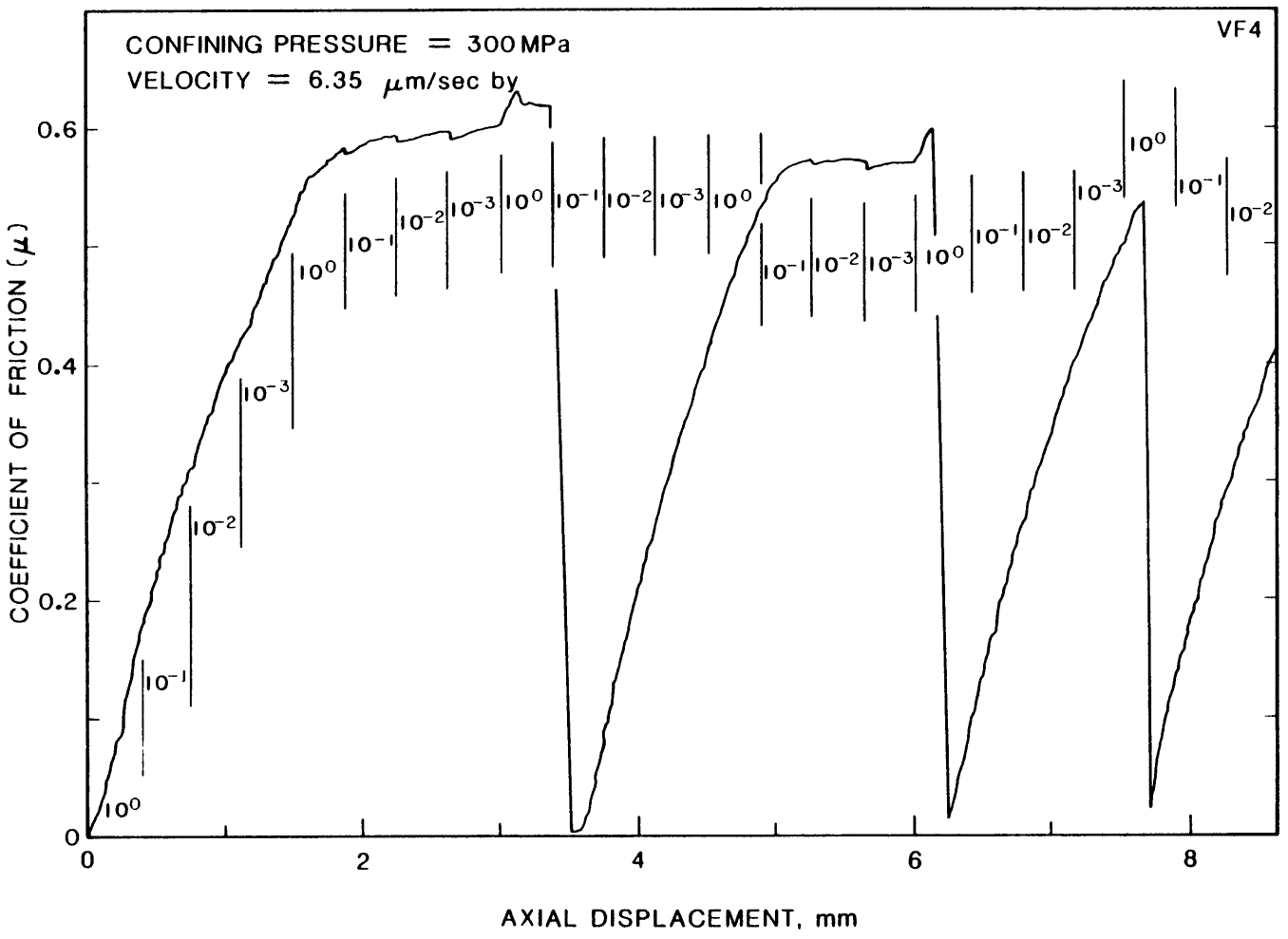
CONFINING PRESSURE = 300 MPa
VELOCITY = 6.35 μm/sec by
VF4
COEFFICIENT OF FRICTION (μ)
AXIAL DISPLACEMENT, mm
0
0.2
0.4
0.6
2
4
6
8
10^0
10^-1
10^-2
10^-3

FIGURE 19

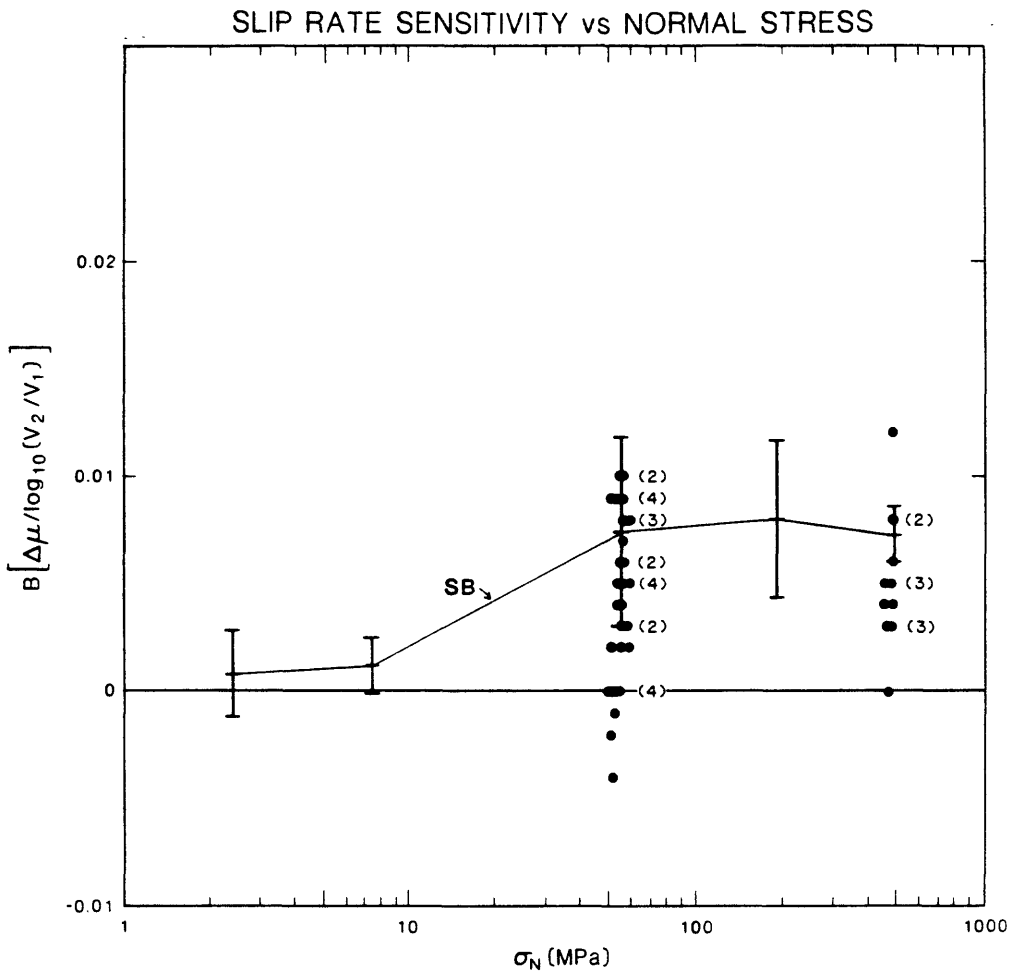
SLIP RATE SENSITIVITY vs NORMAL STRESS
B[Δμ/log10(V2/V1)]
0.02
0.01
0
-0.01
1
10
100
1000
σN (MPa)
SB
(2)
(4)
(3)
(2)
(4)
(2)
(4)
(2)
(3)
(3)

FIGURE 20